NASA CONTRACTOR REPORT

[illegible]
P-50

FLOWFIELD COMPUTATION OF ENTRY VEHICLES

Dinesh K. Prabhu

Eloret Institute
3788 Fabian Way
Palo Alto, CA 94303

Prepared for

Ames Research Center
under Cooperative Agreement NCC2-312

NASA
National Aeronautics and
Space Administration

Ames Research Center
Moffett Field, California 94035

NASA CONTRACTOR REPORT

FLOWFIELD COMPUTATION OF ENTRY VEHICLES

Dinesh K. Prabhu

CONTRACT NAS2–
NCC2-312

1. Report No.	2. Government Accession No.	3. Recipient's Catalog No.
4. Title and Subtitle FLOWFIELD COMPUTATION OF ENTRY VEHICLES		5. Report Date 10 September 1990
		6. Performing Organization Code
7. Author(s) Dinesh K. Prabhu		8. Performing Organization Report No.
		10. Work Unit No.
9. Performing Organization Name and Address Eloret Institute 3788 Fabian Way Palo Alto, CA 94303		11. Contract or Grant No. NCC2-312
		13. Type of Report and Period Covered 6/1/84 to 5/31/90
12. Sponsoring Agency Name and Address National Aeronautics and Space Administration, Washington, D.C. 20456		14. Sponsoring Agency Code

15 Supplementary Notes

Point of Contact: Dr. Dinesh K. Prabhu
c/o 230-2 NASA Ames Research Center, Moffett Field, CA 94035

16. Abstract

The equations governing the multidimensional flow of a reacting mixture of thermally perfect gasses have been derived. The modeling procedures for the various terms of the conservation laws have been discussed. A numerical algorithm, based on the finite-volume approach, to solve these conservation equations has been developed. The advantages and disadvantages of the present numerical scheme have been discussed from the point of view of accuracy, computer time, and memory requirements. A simple one-dimensional model problem has been solved to prove the feasibility and accuracy of the algorithm. A computer code implementing the above algorithm has been developed and is presently being applied to simple geometries and conditions. Once the code is completely debugged and validated, it will be used to compute the complete unsteady flow field around the Aeroassist Flight Experiment (AFE) body.

17. Key Words (Suggested by Author(s)) Multidimensional Flow Finite-Volume Approach Flowfield Entry Vehicles	18. Distribution Statement Unclassified, Unlimited

19. Security Classif. (of this report) Unclassified	20. Security Classif. (of this page) Unclassified	21. No. of Pages	22. Price*

*For sale by the National Technical Information Service, Springfield, Virginia 22161

FLOWFIELD COMPUTATION OF ENTRY VEHICLES

Final Technical Report

for
Cooperative Agreement NCC2-312

for the period
June 1, 1984 - May 31, 1990

Submitted to

National Aeronautics and Space Administration
Ames Research Center
Moffett Field, California 94035

Aerothermodynamics Branch
Dr. George S. Deiwert, Chief and Technical Monitor

Thermosciences Division
Dr. Jim Arnold, Chief

Prepared by

ELORET INSTITUTE
1178 Maraschino Drive
Sunnyvale, CA 94087
Phone: 408 730-8422 and 415 493-4710
Telefax: 408 730-1441
K. Heinemann, President and Grant Administrator
Dinesh K. Prabhu, Principal Investigator

10 September, 1990

Introduction

Work under Cooperative Agreement NCC2-312 was performed in two stages. Stage one commenced on 1 June 1984 and extended through 2/28/87. It was performed under the direction of Dr. Bala A. Balakrishnan as Eloret Principal Investigator; Mr. Mike Green of NASA-Ames Research Center being the Technical Monitor. The final reporting for that stage of the research program was submitted on 31 July, 1987. It included the following five AIAA papers: 85-1006; 85-1064; 85-1063; 86-1277; and 86-1312.

Stage two was performed under the Direction of Dr. Dinesh K. Prabhu during the period 7/1/87 through 5/31/90. Mr. William C. Davy and Dr. George S. Deiwert were the NASA Technical Monitors. This final report concentrates on Dr. Prabhu's work.

Abstract

The equations governing the multidimensional flow of a reacting mixture of thermally perfect gases have been derived. The modelling procedures for the various terms of the conservation laws have been discussed. A numerical algorithm (based on the finite-volume approach) to solve these conservation equations has been developed. The advantages and disadvantages of the present numerical scheme have been discussed from the point of view of accuracy, computer time and memory requirements. A simple one-dimensional model problem has been solved to prove the feasibility and accuracy fo the algorithm. A computer code implementing the above algorithm has been developed and is currently being applied to simple geometries and comditions. Once the code is completely debugged and validated it will be used to compute the complete, unsteady flow field aournd the Aeroassist Flight Experiment (AFE) body.

Nomenclature

$\mathbf{0}$	:	null vector
a_f	:	frozen speed of sound
c_s	:	mass fraction of species s
C_{v_f}	:	frozen specific heat of the mixture
$C_{v,s}$	:	specific heat of species s
$\mathcal{D}$	:	binary diffusion coefficient
E	:	total energy per unit volume of the mixture
e	:	specific internal energy of the mixture
e_s	:	specific internal energy of species s

$\mathbf{F}$	:	algebraic flux vector
$\hat{F}$	:	numerical flux vector
F_n	:	normal component of the flux
H	:	specific total enthalpy of the mixture
h_s^0	:	specific enthalpy of formation of species s
$\mathbf{I}$	:	identity tensor
K_{b_m}	:	backward reaction rate constant for the mth reaction
K_{f_m}	:	forward reaction rate constant for the mth reaction
L	:	reference length (m)
$\mathcal{L}e$	:	binary Lewis number
m	:	number of reactions
M_f	:	frozen Mach number
$\mathcal{M}$	:	molecular weight
n_d	:	number of dimensions
n_e	:	number of conservation equations
n_s	:	number of species
$\mathbf{n}$	:	unit normal to cell surface
p	:	static pressure
$\mathbf{P}$	:	pressure tensor
$\mathbf{q}$	:	heat flux vector
Q	:	algebraic vector of conservative variables
$\mathcal{R}$	:	universal gas constant, 8314.34 $J/(kmol{\cdot}K)$
$\mathbf{r}$	:	position vector
Re	:	Reynolds number based on L
S	:	magnitude of surface area vector
$\mathbf{s}$	:	unit tangent to cell surface

$\mathbf{S}$	:	surface area vector
t	:	time
$\mathbf{t}$	:	unit tangent to cell surface
T	:	temperature
$\mathbf{T}$	:	viscous stress tensor
U	:	algebraic vector of primitive variables
$\mathbf{u}$	:	mass-averaged velocity
u_n	:	velocity component normal to cell surface
V	:	magnitude of the mass-averaged velocity
$\mathcal{V}$	:	cell volume
$\mathbf{V}_s$	:	diffusion velocity of species s
$\mathbf{v}$	:	control surface velocity
$\dot{w}_s$	:	mass production rate of species s
$\dot{W}$	:	vector of production terms
$\hat{W}$	:	numerical representation of the source vector
X_s	:	mole fraction of species s
$[X_s]$	:	molar concentration per unit volume of species s
κ	:	thermal conductivity of the mixture
κ_s	:	thermal conductivity of species s
μ	:	viscosity of the mixture
μ_s	:	viscosity of species s
ρ	:	mass density of the mixture
ρ_s	:	mass density of species s

Subscripts

j, k, l	:	cell centroid indices
$(j, k, l) \pm \frac{1}{2}$	:	cell face indices

n	:	time index
r, s, l	:	indices denoting species
ref	:	reference condition
w	:	wall
∞	:	freestream

Superscripts

$*$	:	dimensional quantity
i	:	inviscid/convective quantity
v	:	viscous/nonconvective quantity
α	:	direction index

Governing Equations

Let $\mathcal{V}$ be the control volume of interest and $\partial\mathcal{V}$ its bounding control surface which moves with a velocity $\mathbf{v}$. The equations governing the flow are[1,2]:

(a) the law of conservation of mass of species s $(s = 1, 2, \ldots, n_s)$:

$$\frac{d}{dt}\int_{\mathcal{V}(t)} \rho_s dV + \oint_{\partial\mathcal{V}(t)} \rho_s(\mathbf{u}-\mathbf{v})\cdot\mathbf{n}dA + \oint_{\partial\mathcal{V}(t)} \rho_s\mathbf{V}_s\cdot\mathbf{n}dA = \int_{\mathcal{V}(t)} \dot{w}_s dV \qquad (1)$$

The first term on the left hand side of Eq. 1 represents the time-rate of change of species mass in the control volume, the second term represents the net flux across the control surface and the third term represents the diffusion mass flux. The term on the right hand side of Eq. 1 represents the rate of mass production/depletion within the control volume. The equation for the overall conservation of mass is obtained by summing Eq. 1 over all the species and noting that

$$\sum_s \rho_s = \rho, \qquad \sum_s \rho_s\mathbf{V}_s = \mathbf{0}, \qquad \sum_s \dot{w}_s = 0$$

Thus, the global continuity equation is

$$\frac{d}{dt}\int_{\mathcal{V}(t)} \rho dV + \oint_{\partial\mathcal{V}(t)} \rho(\mathbf{u}-\mathbf{v})\cdot\mathbf{n}dA = 0$$

(b) the law of conservation of linear momentum:

$$\frac{d}{dt}\int_{\mathcal{V}(t)} \rho\mathbf{u} dV + \oint_{\partial\mathcal{V}(t)} \rho\mathbf{u}(\mathbf{u}-\mathbf{v})\cdot\mathbf{n}dA - \oint_{\partial\mathcal{V}(t)} \mathbf{P}\cdot\mathbf{n}dA = 0 \tag{2}$$

where body forces have been neglected and $\mathbf{P}$ represents the surface forces (stress tensor). The above vector equation leads to n_d scalar equations, where n_d is the number of dimensions.

(c) the law of conservation of energy:

$$\frac{d}{dt}\int_{\mathcal{V}(t)} E dV + \oint_{\partial\mathcal{V}(t)} E(\mathbf{u}-\mathbf{v})\cdot\mathbf{n}dA = -\oint_{\partial\mathcal{V}(t)} \mathbf{q}\cdot\mathbf{n}dA + \oint_{\partial\mathcal{V}(t)} \mathbf{P}\cdot\mathbf{u}\cdot\mathbf{n}dA \tag{3}$$

where E is volumetric total energy of the mixture, and $\mathbf{q}$ is the heat flux vector. The second term on the right hand side of Eq. 3 represents the work done by the surface forces. The volumetric total energy of the mixture is defined as

$$E = \rho(e + \frac{1}{2}\mathbf{u}\cdot\mathbf{u}) \tag{4}$$

We have, therefore, a total of $n_e = n_s + n_d + 1$ conservation equations to solve. The scalar and vector fields of interest to us are ρ_s, ρ, $\mathbf{u}$, p, and T. In order to close the set of governing equations we need to model the various terms appearing in the set. This is discussed in the following section.

Physical Model

(a) thermal equation of state:

The constituent gases of the mixture are assumed to be thermally perfect and obey the following equation of state for the partial pressure p_s

$$p_s = \frac{\rho_s \mathcal{R} T}{\mathcal{M}_s}$$

Using Dalton's law of partial pressures, the following equation of state is obtained for the mixture

$$p = \frac{\rho \mathcal{R} T}{\mathcal{M}} \tag{5}$$

where $\mathcal{M}$ is the molecular weight of the mixture and is defined as

$$\mathcal{M} = \left(\sum_s \frac{c_s}{\mathcal{M}_s} \right)^{-1} \tag{7}$$

(b) thermodynamic properties:

The thermodynamic properties of the individual species of the gas are available as cubic-spline fits. These curve fits are of the form

$$e_s = e_s(T) + h_s^0 = a_0 + a_1 T + a_2 T^2 + a_3 T^3$$

$$C_{v_s} = C_{v_s}(T) = \frac{de_s}{dT} = a_1 + 2a_2 T + 3a_3 T^2$$

where $a_0, \ldots, a_3$ are the spline coefficients. These coefficients have been generated by Liu and Vinokur[3] and based on quantum calculations done by Jaffe[4]. These thermodynamic properties are considered more realistic than previous calculations because they account for the internal structure of the atoms and molecules. The thermodynamic properties of mixture as a whole are computed as simple weighted sums of the individual species properties, *i.e.*,

$$C_{v_f} = \sum_s c_s C_{v_s} \qquad e = \sum_s c_s e_s \tag{8}$$

(c) <u>transport properties</u>:

The viscosities of the individual species are computed using curve fits developed by Blottner *et al.*[5] and these are of the form

$$\mu_s = \exp[(a \log_e T + b) \log_e T + c]$$

where a, b, c are constants. The thermal conductivities of the individual species are computed using Eucken's formula

$$\kappa_s = \frac{\mu_s \mathcal{R}}{\mathcal{M}_s}(\frac{C_{v_s}\mathcal{M}_s}{\mathcal{R}} + 2.25)$$

The transport properties of the mixture are calculated using Wilke's mixing rule.[6] This mixing rule, considered adequate for weakly ionizing flows, is mathematically expressed as

$$\mu = \sum_{s=1}^{n} \frac{X_s \mu_s}{\phi_s}, \qquad \kappa = \sum_{s=1}^{n} \frac{X_s \kappa_s}{\phi_s} \tag{9}$$

where

$$X_s = \frac{c_s \mathcal{M}}{\mathcal{M}_s}$$

$$\phi_s = \sum_{r=1}^{n} X_r \left[1 + \sqrt{\frac{\mu_s}{\mu_r}} \left(\frac{\mathcal{M}_r}{\mathcal{M}_s}\right)^{1/4}\right]^2 \left[\sqrt{8}\sqrt{1 + \frac{\mathcal{M}_s}{\mathcal{M}_r}}\right]^{-1}$$

The binary diffusion coefficient is obtained from the definition of the Lewis number, $\mathcal{L}e$, which is assumed to be the same for all species. Therefore,

$$\mathcal{D} = \frac{\kappa \mathcal{L}e}{\rho C_{p_f}} \tag{10}$$

(d) diffusion mass flux:

Assuming the thermal and pressure diffusion effects to be negligible and that mass diffusion is binary, the diffusion mass flux can be expressed as

$$\rho_s \mathbf{V}_s = -\rho \mathcal{D} \nabla c_s \tag{11}$$

The binary diffusion approximation is valid for mildly ionizing air consisting of "heavy" particles (molecules and ions) and "light" particles (atoms). This assumption considerably simplifies the complexities of a true multicomponent diffusion model.

(e) stress tensor:

Bulk viscosity effects are considered to be negligibly small. The stress tensor represented as the sum of the hydrostatic and deviatoric stress is written as

$$\mathbf{P} = -p\mathbf{I} + \mathbf{T} = -p\mathbf{I} + \mu[\nabla \mathbf{u} + (\nabla \mathbf{u})^T - \frac{2}{3}\nabla \cdot \mathbf{u}\mathbf{I}] \tag{12}$$

where μ is the coefficient of viscosity, $\mathbf{I}$ is the identity tensor, and ∇ is the usual gradient operator.

(f) heat flux vector:

The heat flux vector consists of two parts, (i) a conduction part and (ii) a diffusion part. This is expressed as

$$\mathbf{q} = -\kappa \nabla T + \sum_s h_s \rho_s \mathbf{V}_s \tag{13}$$

where κ is the coefficient of thermal conductivity. The heat transfer due to radiation has been neglected.

(g) chemical production terms:

Consider the chemical reactions

$$\sum_s \nu'_{k,s} A_s \rightleftharpoons \sum_s \nu''_{k,s} A_s \qquad k = 1, 2, \ldots, m$$

where A_s represents the species s. Then the mass-production rate of species s is

$$\dot{w}_s = \mathcal{M}_s \sum_k (\nu''_{k,s} - \nu'_{k,s}) \left\{ K_{f_k}(T) \prod_l [X_l]^{\nu'_{k,l}} - K_{b_k}(T) \prod_l [X_l]^{\nu''_{k,l}} \right\} \tag{14}$$

where the forward and backward production rates are expressed in the modified Arrhenius form as

$$\begin{aligned} K_{f_k}(T) &= \exp(C_{0,k} + \frac{C_{1,k}}{T} + C_{2,k} \log_e T) \\ K_{f_k}(T) &= \exp(D_{0,k} + \frac{D_{1,k}}{T} + D_{2,k} \log_e T) \end{aligned}$$

where $C_{0,k}, \ldots, D_{2,k}$ are given constants.[5]

Nondimensionalization

All the physical quantities appearing in the preceding equations are nondimensionalized using their reference values. These reference values (dimensional quantities being denoted by *) are defined as:

$$\begin{array}{llll} |\mathbf{r}^*|_{ref} = L^* & \mathcal{M}^*_{ref} = \mathcal{M}^*_\infty & e^*_{ref} = V^{*2}_{ref} & \kappa^*_{ref} = \mu^*_{ref} R^*_{ref} \\ V^*_{ref} = V^*_\infty & R^*_{ref} = \dfrac{\mathcal{R}}{\mathcal{M}^*_{ref}} & C^*_{v,ref} = R^*_{ref} & \mathcal{D}^*_{ref} = \dfrac{\mu^*_{ref}}{\rho^*_{ref}} \\ t^*_{ref} = \dfrac{|\mathbf{r}^*|_{ref}}{V^*_{ref}} & T^*_{ref} = \dfrac{V^{*2}_{ref}}{R^*_{ref}} & \mu^*_{ref} = \mu^*_\infty & \dot{w}^*_{ref} = \dfrac{\rho^*_{ref} V^*_{ref}}{L^*} \\ \rho^*_{ref} = \rho^*_\infty & p^*_{ref} = \rho^*_{ref} V^{*2}_{ref} & & \end{array} \tag{15}$$

and the other nondimensional parameter of interest is the Reynolds number which is defined as

$$Re = \frac{\rho^*_{ref} V^*_{ref} L^*}{\mu^*_{ref}}$$

The equations Eq. 1, 2, and 3 along with the equations Eqs. 4-14 provide a complete set of equations for the unlnown fields ρ_s, ρ, $\mathbf{u}$, p, and T. These equations are discretized using the finite-volume approach which is discussed next.

Discretization

(a) Preliminaries:

The conservation equations, Eqs. 1, 2, 3 can be written as one single equation in nondimensional integral form as

$$\frac{d}{dt}\int_{\mathcal{V}(t)} Q dV + \oint_{\partial\mathcal{V}(t)} \mathbf{F}\cdot\mathbf{n} dA = \int_{\mathcal{V}(t)} \dot{W} dV \tag{16}$$

where the vector of dependent conservative variables, Q, is:

$$Q = \{\rho_1, \rho_2, \ldots, \rho_{n_s}, \rho\mathbf{u}, E\}^T \tag{17}$$

$$\mathbf{F} = \mathbf{F}^i - \mathbf{F}^v = \begin{pmatrix} \rho_1(\mathbf{u}-\mathbf{v}) \\ \rho_2(\mathbf{u}-\mathbf{v}) \\ \vdots \\ \rho_{n_s}(\mathbf{u}-\mathbf{v}) \\ \rho\mathbf{u}(\mathbf{u}-\mathbf{v}) + p\mathbf{I} \\ E(\mathbf{u}-\mathbf{v}) + p\mathbf{u} \end{pmatrix} - \frac{1}{Re}\begin{pmatrix} \rho\mathcal{D}\nabla c_1 \\ \rho\mathcal{D}\nabla c_2 \\ \vdots \\ \rho\mathcal{D}\nabla c_{n_s} \\ \mathbf{T} \\ \mathbf{T}\cdot\mathbf{u} - \mathbf{q} \end{pmatrix} \quad \dot{W} = \begin{pmatrix} \dot{w}_1 \\ \dot{w}_2 \\ \vdots \\ \dot{w}_{n_s} \\ \mathbf{0} \\ 0 \end{pmatrix} \tag{18}$$

Let the $\mathbf{n}$ be the unit vector normal to the control surface. Further, let $F_n = \mathbf{n}\cdot\mathbf{F}$ be the normal component of the algebraic flux vector and let $u_n = \mathbf{n}\cdot\mathbf{u}$, $v_n = \mathbf{n}\cdot\mathbf{v}$, $u'_n = u_n - v_n$ be respectively, the flow, the control surface, and the relative velocity components normal to the control surface. The normal component of the inviscid flux vector is:

$$F_n^i(Q;\mathbf{n}) = \mathbf{n}\cdot\mathbf{F}^i = \{\rho_1 u_n', \rho_2 u_n', \ldots, \rho_{n_s} u_n', \rho u_n' \mathbf{u} + p\mathbf{n}, E u_n' + p u_n\}^T$$

In many numerical algorithms, the above nonlinear flux vector is often linearized in time or space. This linearization leads to the following $n_e \times n_e$ inviscid Jacobian matrix

$$\mathbf{A}^i(U;\mathbf{n}) = \begin{pmatrix} u_n'\delta_{rs} - c_r u_n & c_r\mathbf{n} & 0 \\ \overline{\gamma}(\frac{1}{2}\mathbf{u}\cdot\mathbf{u} + \psi_s)\mathbf{n} - u_n\mathbf{u} & \mathbf{u}\mathbf{n} - \overline{\gamma}\mathbf{n}\mathbf{u} + u_n'\mathbf{I} & \overline{\gamma}\mathbf{n} \\ [\overline{\gamma}(\frac{1}{2}\mathbf{u}\cdot\mathbf{u} + \psi_s) - H]u_n & H\mathbf{n} - \overline{\gamma}u_n\mathbf{u} & u_n' + \overline{\gamma}u_n \end{pmatrix} \qquad (19)$$

where δ_{rs} is the Kronecker delta with $r, s = 1, 2, \ldots, n_s$ and

$$\overline{\gamma} = \frac{1}{\mathcal{M}C_{v_f}} \qquad \psi_s = \frac{C_{v_f}T\mathcal{M}}{\mathcal{M}_s} - e_s \qquad (20)$$

U is the vector of primitive variables $\rho_s, \rho, \mathbf{u}, p, \ldots$. The eigenvalues of this inviscid Jacobian matrix are:

$$\begin{aligned} \lambda_i &= u_n' \quad i = 1, 2, \ldots, n_s + n_d - 1 \\ \lambda_{n_s+n_d} &= u_n' - a_f \\ \lambda_{n_s+n_d+1} &= u_n' + a_f \end{aligned} \qquad (21)$$

where the frozen speed of sound a_f is defined as

$$a_f = \sqrt{(1+\overline{\gamma})\frac{p}{\rho}} \qquad (22)$$

Define the unit tangent vectors **s**, **t** such that $\mathbf{n}, \mathbf{s}, \mathbf{t}$ form a unit orthonormal spatial basis, *i.e.*,

$$\mathbf{n}\cdot\mathbf{s} = \mathbf{n}\cdot\mathbf{t} = \mathbf{s}\cdot\mathbf{t} = 0 \qquad |\mathbf{n}| = |\mathbf{s}| = |\mathbf{t}| = 1$$

The Jacobian matrix $\mathbf{A}$ can also be written as $\mathbf{A} = \mathbf{R}\Lambda\mathbf{L}$, where Λ is a diagonal matrix of eigenvalues of $\mathbf{A}$,

$$\Lambda(U;\mathbf{n}) = \mathrm{diag}\left\{u_n', u_n', \ldots, u_n', u_n' - a_f, u_n' + a_f\right\}^T \tag{23}$$

and $\mathbf{L}$ and $\mathbf{R}$ are the left and right eigenvector matrices, respectively.

$$\mathbf{R}(U;\mathbf{n},\mathbf{s},\mathbf{t}) = \begin{pmatrix} \delta_{rs} & 0 & 0 & c_r & c_r \\ \mathbf{u} & a_f\mathbf{t} & a_f\mathbf{s} & \mathbf{u} - a_f\mathbf{n} & \mathbf{u} + a_f\mathbf{n} \\ \frac{1}{2}\mathbf{u}\cdot\mathbf{u} - \psi_s & a_f\mathbf{u}\cdot\mathbf{t} & a_f\mathbf{u}\cdot\mathbf{s} & H - a_f u_n & H + a_f u_n \end{pmatrix} \tag{24}$$

$$\mathbf{L}(U;\mathbf{n},\mathbf{s},\mathbf{t}) = \frac{1}{2a_f{}^2}\begin{pmatrix} 2a_f{}^2\delta_{rs} - 2c_r\overline{\gamma}(\frac{1}{2}\mathbf{u}\cdot\mathbf{u} + \psi_s) & 2c_r\overline{\gamma}\mathbf{u} & -2c_r\overline{\gamma} \\ -2a_f\mathbf{u}\cdot\mathbf{t} & 2a_f\mathbf{t} & 0 \\ -2a_f\mathbf{u}\cdot\mathbf{s} & 2a_f\mathbf{s} & 0 \\ \overline{\gamma}(\frac{1}{2}\mathbf{u}\cdot\mathbf{u} + \psi_s) + a_f u_n & -\overline{\gamma}\mathbf{u} - a_f\mathbf{n} & \overline{\gamma} \\ \overline{\gamma}(\frac{1}{2}\mathbf{u}\cdot\mathbf{u} + \psi_s) - a_f u_n & -\overline{\gamma}\mathbf{u} + a_f\mathbf{n} & \overline{\gamma} \end{pmatrix} \tag{25}$$

Columns 2 and 3 of $\mathbf{R}$ and rows 2 and 3 of $\mathbf{L}$ can be dropped for the case of a one-dimensional flow. Column 3 of $\mathbf{R}$ and row 3 of $\mathbf{L}$ can be dropped for the case of a two-dimensional flow.

(b) Spatial Discretization:

In this research effort, the finite-volume method[7] is chosen to discretize the governing equations. In the finite-volume method the flow domain is divided into contiguous cells and the conservation principles applied to each of these cells. This in effect replaces the surface integrals in Eq. 16 by the sum of integrals over the faces of the cells. For the case of three dimensional flow, the cells are hexahedra defined by specifying the vertices $\mathbf{r}_{j\pm\frac{1}{2},k\pm\frac{1}{2},l\pm\frac{1}{2}}$ (whole indices represent the cell centroid or cell center) and these vertices are used to compute the surface area vectors and cell volumes. In the interpretation of the volume integrals, the state of dependent variables is assumed to be the value of Q at some average point in the cell, *e.g.*, the cell center. For a hexahedral cell (see Fig. 1) centered at j, k, l, the semi-discrete version of Eq. 8 can be written as

$$\mathcal{V}_{j,k,l}\frac{d}{dt}Q_{j,k,l} + \sum_{\alpha=1}^{n_d} \hat{F}^{\alpha}_{m_\alpha+\frac{1}{2}} - \hat{F}^{\alpha}_{m_\alpha-\frac{1}{2}} = \mathcal{V}_{j,k,l}\hat{W}_{j,k,l} \tag{26}$$

m_α represents either j, or k, or l according to whether α is 1, or 2, or 3. In any case the index m_α is always an integer. The circumflex above the flux and source vectors indicates that these are numerical quantities. These are consistent with the physical fluxes and source vectors. For example, if the numerical flux vector $\hat{F}^\alpha$ is defined as:

$$\hat{F}^{\alpha}_{m_\alpha+\frac{1}{2}} = \hat{F}^{\alpha}(Q_{m_\alpha+2}, Q_{m_\alpha+1}, Q_{m_\alpha}, Q_{m_\alpha-1}; \mathbf{S}^{\alpha}_{m_\alpha+\frac{1}{2}})$$

then the consistency requirement is simply

$$\hat{F}^{\alpha}(Q_{m_\alpha}, Q_{m_\alpha}, Q_{m_\alpha}, Q_{m_\alpha}; \mathbf{S}^{\alpha}_{m_\alpha+\frac{1}{2}}) = \mathbf{S}^{\alpha}_{m_\alpha+\frac{1}{2}} \cdot \mathbf{F}(Q_{m_\alpha})$$

The required surface area vectors of the cell faces are computed using the formulas below[7]

$$\begin{aligned}
\mathbf{S}^{\xi}_{j\pm\frac{1}{2},k,l} &= \frac{1}{2}(\mathbf{r}_{j\pm\frac{1}{2},k+\frac{1}{2},l-\frac{1}{2}} - \mathbf{r}_{j\pm\frac{1}{2},k-\frac{1}{2},l+\frac{1}{2}}) \otimes (\mathbf{r}_{j\pm\frac{1}{2},k+\frac{1}{2},l+\frac{1}{2}} - \mathbf{r}_{j\pm\frac{1}{2},k-\frac{1}{2},l-\frac{1}{2}}) \\
\mathbf{S}^{\eta}_{j,k\pm\frac{1}{2},l} &= \frac{1}{2}(\mathbf{r}_{j+\frac{1}{2},k\pm\frac{1}{2},l-\frac{1}{2}} - \mathbf{r}_{j-\frac{1}{2},k\pm\frac{1}{2},l+\frac{1}{2}}) \otimes (\mathbf{r}_{j-\frac{1}{2},k\pm\frac{1}{2},l-\frac{1}{2}} - \mathbf{r}_{j+\frac{1}{2},k\pm\frac{1}{2},l+\frac{1}{2}}) \\
\mathbf{S}^{\zeta}_{j,k,l\pm\frac{1}{2}} &= \frac{1}{2}(\mathbf{r}_{j+\frac{1}{2},k+\frac{1}{2},l\pm\frac{1}{2}} - \mathbf{r}_{j-\frac{1}{2},k-\frac{1}{2},l\pm\frac{1}{2}}) \otimes (\mathbf{r}_{j-\frac{1}{2},k+\frac{1}{2},l\pm\frac{1}{2}} - \mathbf{r}_{j+\frac{1}{2},k-\frac{1}{2},l\pm\frac{1}{2}})
\end{aligned} \tag{27}$$

and the cell volume is computed using the formula[7]

$$\mathcal{V}_{j,k,l} = \frac{1}{3}(\mathbf{r}_{j+\frac{1}{2},k+\frac{1}{2},l+\frac{1}{2}} - \mathbf{r}_{j-\frac{1}{2},k-\frac{1}{2},l-\frac{1}{2}}) \cdot (\mathbf{S}^{\xi}_{j-\frac{1}{2},k,l} + \mathbf{S}^{\eta}_{j,k-\frac{1}{2},l} + \mathbf{S}^{\zeta}_{j,k,l-\frac{1}{2}}) \tag{28}$$

There are two ways of obtaining second and higher order representation of the inviscid numerical flux at a call face. In the first approach, the cell centroid values at the neighboring cells are used to set up a Riemann problem at the face under consideration and this is called the MUSCL (Monotonic Upwind Schemes for Conservation Laws) approach. This approach is closer to the spirit of the finite-volume formulation. In the second approach, the physical fluxes at computed at the neighboring cell centers and then used in a weighted manner. This approach is called the non-MUSCL approach approach. Both these approaches are discussed below.

(i) Inviscid Fluxes - MUSCL representation

In the MUSCL approach[15] the piecewise constant initial data of the Riemann problem in Godunov's method[16] are replaced with piecewise linear inital data. The required right (R) and left (L) states of the Riemann problem at the face $j+\frac{1}{2}$ are defined as

$$Q^R_{m_\alpha+\frac{1}{2}} = Q_{m_\alpha+1} - \left[\frac{1-\phi}{4}(Q_{m_\alpha+2} - Q_{m_\alpha+1}) + \frac{1+\phi}{4}(Q_{m_\alpha+1} - Q_{m_\alpha})\right]$$
$$Q^L_{m_\alpha+\frac{1}{2}} = Q_{m_\alpha} + \left[\frac{1-\phi}{4}(Q_{m_\alpha} - Q_{m_\alpha-1}) + \frac{1+\phi}{4}(Q_{m_\alpha+1} - Q_{m_\alpha})\right]$$

The parameter ϕ determines the spatial order of accuracy. For example, $\phi = -1$ leads to a fully upwind scheme and $\phi = \frac{1}{3}$ leads to a third-order upwind-biased scheme. The left and right states as defined above lead to nonphysical oscillations at discontinuities. In order to eliminate these oscillations we define the following intermediate vectors

$$\chi_{1,m_\alpha+\frac{1}{2}} = (Q_{m_\alpha+2} - Q_{m_\alpha+1})$$
$$\chi_{2,m_\alpha+\frac{1}{2}} = (Q_{m_\alpha+1} - Q_{m_\alpha})$$
$$\chi_{3,m_\alpha+\frac{1}{2}} = (Q_{m_\alpha} - Q_{m_\alpha-1})$$

The elements of these intermediate vectors are then limited relative to each other. The limited vectors are given by

$$\overline{\chi}_{1,m_\alpha+\frac{1}{2}} = \text{minmod}(\chi_{1,m_\alpha+\frac{1}{2}}, b\chi_{2,m_\alpha+\frac{1}{2}})$$
$$\overline{\chi}_{2,m_\alpha+\frac{1}{2}} = \text{minmod}(\chi_{2,m_\alpha+\frac{1}{2}}, b\chi_{3,m_\alpha+\frac{1}{2}})$$
$$\overline{\overline{\chi}}_{2,m_\alpha+\frac{1}{2}} = \text{minmod}(\chi_{2,m_\alpha+\frac{1}{2}}, b\chi_{1,m_\alpha+\frac{1}{2}})$$
$$\overline{\overline{\chi}}_{3,m_\alpha+\frac{1}{2}} = \text{minmod}(\chi_{3,m_\alpha+\frac{1}{2}}, b\chi_{2,m_\alpha+\frac{1}{2}})$$

where the limiting operator is defined by

$$\text{minmod}(x, by) = \text{sgn}(x) \max\{0, \min[|x|, by\text{sgn}(x)]\}$$

and $1 \leq b \leq (3-\phi)/(1-\phi)$ and $\phi \neq 1$. In terms of these limited intermediate vectors, the limited left and right states at a cell face are

$$Q^R_{m_\alpha+\frac{1}{2}} = Q_{m_\alpha+1} - \left[\frac{1-\phi}{4}\overline{\chi}_{1,m_\alpha+\frac{1}{2}} + \frac{1+\phi}{4}\overline{\overline{\chi}}_{2,m_\alpha+\frac{1}{2}}\right]$$
$$Q^L_{m_\alpha+\frac{1}{2}} = Q_{m_\alpha} + \left[\frac{1-\phi}{4}\overline{\overline{\chi}}_{3,m_\alpha+\frac{1}{2}} + \frac{1+\phi}{4}\overline{\chi}_{2,m_\alpha+\frac{1}{2}}\right]$$

Using these limited states in the first-order Roe scheme[10] we obtain the higher-order inviscid numerical flux

$$\hat{F}^{\alpha,i}_{m_\alpha+\frac{1}{2}} = \frac{1}{2}\left\{\mathbf{S}^\alpha_{m_\alpha+\frac{1}{2}} \cdot [\mathbf{F}^i(Q^R_{m_\alpha+\frac{1}{2}}) + \mathbf{F}^i(Q^L_{m_\alpha+\frac{1}{2}})] - |\mathbf{A}^{\alpha,i}_{m_\alpha+\frac{1}{2}}|(Q^R_{m_\alpha+\frac{1}{2}} - Q^L_{m_\alpha+\frac{1}{2}})\right\} \quad (29)$$

where

$$|\mathbf{A}^{\alpha,i}_{m_\alpha+\frac{1}{2}}| = S^\alpha_{m_\alpha+\frac{1}{2}}\mathbf{R}^\alpha_{m_\alpha+\frac{1}{2}}|\Lambda^\alpha_{m_\alpha+\frac{1}{2}}|\mathbf{L}^\alpha_{m_\alpha+\frac{1}{2}} \quad (30)$$

and the elements of the diagonal matrix $|\Lambda|$ are

$$|(\lambda^{\alpha}_{m_\alpha+\frac{1}{2}})_\ell| = \psi[(\lambda^{\alpha}_{m_\alpha+\frac{1}{2}})_\ell] \quad \ell = 1, 2, \ldots, n_e$$

The function $\psi[z]$ is necessary to prevent entropy-violating expansion shocks and defined as[11]

$$\psi[z] = \begin{cases} |z| & |z| \geq \epsilon \\ (z^2 + \epsilon^2)/2\epsilon & |z| < \epsilon \end{cases} \tag{31}$$

and ϵ is some small positive parameter. This function is required at points where the eigenvalue goes to zero. The superscript α on $\mathbf{L}$, $\mathbf{R}$, and Λ indicates that these matrices are evaluated using the basis vectors $\mathbf{n}, \mathbf{s}, \mathbf{t}$ for the α-direction and the subscript $m_\alpha + \frac{1}{2}$ indicates that an averaged state at the cell face is used in the evaluation. This averaged state is some symmetric average of the limited left and right states. Note that the spatial differencing stencil consists of five points.

(ii) Inviscid Fluxes - Non-MUSCL representation

(1) Osher-Chakravarthy:

The first-order accurate inviscid numerical flux $\hat{F}^{\alpha,i}_{m_\alpha+\frac{1}{2}}$ is written as[10]

$$\left.\hat{F}^{\alpha,i}_{m_\alpha+\frac{1}{2}}\right|_{FO} = \frac{1}{2}\left\{\mathbf{S}^{\alpha}_{m_\alpha+\frac{1}{2}} \cdot \left[\mathbf{F}^i(Q_{m_\alpha+1}) + \mathbf{F}^i(Q_{m_\alpha})\right] - |\mathbf{A}^{\alpha,i}_{m_\alpha+\frac{1}{2}}|(Q_{m_\alpha+1} - Q_{m_\alpha})\right\} \tag{32}$$

which is actually the average of two one-sided representations

$$\begin{aligned} \left.\hat{F}^{\alpha,i}_{m_\alpha+\frac{1}{2}}\right|_{FO} &= \mathbf{S}^{\alpha}_{m_\alpha+\frac{1}{2}} \cdot \mathbf{F}^i(Q_{m_\alpha}) + \mathbf{A}^{\alpha,i-}_{m_\alpha+\frac{1}{2}}(Q_{m_\alpha+1} - Q_{m_\alpha}) \\ \left.\hat{F}^{\alpha,i}_{m_\alpha+\frac{1}{2}}\right|_{FO} &= \mathbf{S}^{\alpha}_{m_\alpha+\frac{1}{2}} \cdot \mathbf{F}^i(Q_{m_\alpha+1}) - \mathbf{A}^{\alpha,i+}_{m_\alpha+\frac{1}{2}}(Q_{m_\alpha+1} - Q_{m_\alpha}) \end{aligned} \tag{33}$$

where $|\mathbf{A}|$ is defined in Eq. 30 and the matrices $\mathbf{A}^{\pm}$ are

$$\mathbf{A}^{\alpha,i\pm}_{m_\alpha+\frac{1}{2}} = S^{\alpha}_{m_\alpha+\frac{1}{2}} \mathbf{R}^{\alpha}_{m_\alpha+\frac{1}{2}} \Lambda^{\alpha\pm}_{m_\alpha+\frac{1}{2}} \mathbf{L}^{\alpha}_{m_\alpha+\frac{1}{2}}$$

The elements of the diagonal matrices $\Lambda^{\pm}$ are

$$(\lambda^{\alpha,\pm}_{m_\alpha+\frac{1}{2}})_\ell = \frac{1}{2}\left\{(\lambda^{\alpha}_{m_\alpha+\frac{1}{2}})_\ell \pm \psi[(\lambda^{\alpha}_{m_\alpha+\frac{1}{2}})_\ell]\right\} \quad \ell = 1, 2, \ldots, n_e$$

where the function $\psi[z]$ is defined in Eq. 31.

In order to improve the spatial accuracy to second order the following intermediate algebraic vectors (characteristic variables) are defined[3]

$$\chi^{\alpha}_{1,m_\alpha+\frac{1}{2}} = \mathbf{L}^{\alpha}_{m_\alpha+\frac{1}{2}}(Q_{m_\alpha+2} - Q_{m_\alpha+1})$$
$$\chi^{\alpha}_{2,m_\alpha+\frac{1}{2}} = \mathbf{L}^{\alpha}_{m_\alpha+\frac{1}{2}}(Q_{m_\alpha+1} - Q_{m_\alpha})$$
$$\chi^{\alpha}_{3,m_\alpha+\frac{1}{2}} = \mathbf{L}^{\alpha}_{m_\alpha+\frac{1}{2}}(Q_{m_\alpha} - Q_{m_\alpha-1})$$

As before, to prevent nonphysical oscillations at shocks, the elements of these intermediate vectors are limited relative to each other. The limited vectors are

$$\overline{\chi}^{\alpha}_{1,m_\alpha+\frac{1}{2}} = \text{minmod}(\chi^{\alpha}_{1,m_\alpha+\frac{1}{2}}, b\chi^{\alpha}_{2,m_\alpha+\frac{1}{2}})$$
$$\overline{\chi}^{\alpha}_{2,m_\alpha+\frac{1}{2}} = \text{minmod}(\chi^{\alpha}_{2,m_\alpha+\frac{1}{2}}, b\chi^{\alpha}_{3,m_\alpha+\frac{1}{2}})$$
$$\overline{\overline{\chi}}^{\alpha}_{2,m_\alpha+\frac{1}{2}} = \text{minmod}(\chi^{\alpha}_{2,m_\alpha+\frac{1}{2}}, b\chi^{\alpha}_{1,m_\alpha+\frac{1}{2}})$$
$$\overline{\overline{\chi}}^{\alpha}_{3,m_\alpha+\frac{1}{2}} = \text{minmod}(\chi^{\alpha}_{3,m_\alpha+\frac{1}{2}}, b\chi^{\alpha}_{2,m_\alpha+\frac{1}{2}})$$

In terms of these limited fluxes, the higher order inviscid flux can be written as[12]

$$\hat{F}^{\alpha,i}_{m_\alpha+\frac{1}{2}} = \hat{F}^{\alpha,i}_{m_\alpha+\frac{1}{2}}\Big|_{FO} - \frac{1-\phi}{4}\mathbf{R}^{\alpha}_{m_\alpha+\frac{1}{2}}\Lambda^{\alpha,-}_{m_\alpha+\frac{1}{2}}\overline{\chi}^{\alpha}_{1,m_\alpha+\frac{1}{2}} - \frac{1+\phi}{4}\mathbf{R}^{\alpha}_{m_\alpha+\frac{1}{2}}\Lambda^{\alpha,-}_{m_\alpha+\frac{1}{2}}\overline{\overline{\chi}}^{\alpha}_{2,m_\alpha+\frac{1}{2}}$$
$$+\frac{1-\phi}{4}\mathbf{R}^{\alpha}_{m_\alpha+\frac{1}{2}}\Lambda^{\alpha,+}_{m_\alpha+\frac{1}{2}}\overline{\overline{\chi}}^{\alpha}_{3,m_\alpha+\frac{1}{2}} + \frac{1+\phi}{4}\mathbf{R}^{\alpha}_{m_\alpha+\frac{1}{2}}\Lambda^{\alpha,+}_{m_\alpha+\frac{1}{2}}\overline{\chi}^{\alpha}_{2,m_\alpha+\frac{1}{2}} \tag{34}$$

The parameter ϕ has the same meaning as in the MUSCL approach. Again, the matrices $\mathbf{R}$, $\mathbf{L}$, and Λ are evaluated at some averaged state at the cell face. This averaging could be done using Roe averaging procedure or even a simple arithmetic averaging procedure. Roe-averaging in the context of nonequilibrium is a little difficult since we can only satisfy either the jump condition or the jump condition but not both simultaneously. In the present work simple arithmetic averaging is used. Note that the spatial differencing stencil again consists of five points.

(2) Harten:

In this method of representing the numerical flux, the concept of a modified flux is used. In terms of this modified flux[11], the second-order accurate inviscid numerical flux $\hat{F}^{\alpha,i}_{m_\alpha+\frac{1}{2}}$ is written as[2]

$$\hat{F}^{\alpha,i}_{m_\alpha+\frac{1}{2}}\Big|_{HO} = \frac{1}{2}\left\{\mathbf{S}^{\alpha}_{m_\alpha+\frac{1}{2}} \cdot \left[\mathbf{F}^i(Q_{m_\alpha+1}) + \mathbf{F}^i(Q_{m_\alpha})\right] + S^{\alpha}_{m_\alpha+\frac{1}{2}}\mathbf{R}^{\alpha}(Q_{m_\alpha+\frac{1}{2}})\Phi^{\alpha}_{m_\alpha+\frac{1}{2}}\right\} \qquad (35)$$

The elements of the vector Φ are

$$\phi^{\alpha,l}_{m_\alpha+\frac{1}{2}} = \frac{1}{2}\psi(\lambda^{\alpha,l}_{m_\alpha+\frac{1}{2}})(g^{\alpha,l}_{m_\alpha+1} + g^{\alpha,l}_{m_\alpha}) - \psi(\lambda^{\alpha,l}_{m_\alpha+\frac{1}{2}} + \gamma^{\alpha,l}_{m_\alpha+\frac{1}{2}})\chi^{\alpha,l}_{m_\alpha+\frac{1}{2}}$$

where g^l is the lth element of the modified flux g and χ^l the lth element of the characteristic variable χ. As before the characteristic variable is defined as

$$\chi_{m_\alpha+\frac{1}{2}} = \mathbf{L}^{\alpha}(Q_{m_\alpha+\frac{1}{2}})(Q_{m_\alpha+1} - Q_{m_\alpha})$$

In the expression for the flux, the modified eigenvalue γ^l is

$$\gamma^l_{m_\alpha+\frac{1}{2}} = \frac{1}{2}\psi(\lambda^l_{m_\alpha+\frac{1}{2}})\begin{cases}(g^l_{m_\alpha+1} - g^l_{m_\alpha})/\alpha^l_{m_\alpha+\frac{1}{2}} & \alpha^l_{m_\alpha+\frac{1}{2}} \neq 0\\ 0 & \alpha^l_{m_\alpha+\frac{1}{2}} = 0\end{cases}$$

and the modified flux is

$$g^l_{m_\alpha} = \text{minmod}(\alpha^l_{m_\alpha - \frac{1}{2}}, \alpha^l_{m_\alpha + \frac{1}{2}})$$

Note that in this representation, we can achieve second-order accuracy in both space and time. This scheme, however, is a little more dissipative than the other two schemes that have been outlined in the preceding sections.

(iii) Viscous Fluxes

The computation of the viscous part of the numerical flux involves the evaluation of the stress tensor and heat flux vector at the cell interfaces, *i.e.*, we have to compute $\mathbf{T}_{m_\alpha \pm \frac{1}{2}}$, $\mathbf{q}_{m_\alpha \pm \frac{1}{2}}$. First consider the viscous stress tensor $\mathbf{T}_{m_\alpha + \frac{1}{2}}$. This can be written as

$$\mathbf{T}_{m_\alpha + \frac{1}{2}} = \mu_{m_\alpha + \frac{1}{2}} \left[(\nabla \mathbf{u})_{m_\alpha + \frac{1}{2}} + (\nabla \mathbf{u})^T_{m_\alpha + \frac{1}{2}} - \frac{2}{3} (\nabla \cdot \mathbf{u})_{m_\alpha + \frac{1}{2}} \mathbf{I} \right] \tag{36}$$

In order to evaluate the terms indicated in the parentheses, we use the divergence theorem.[7] For an arbitrary field $\mathbf{a}$ (scalar or vector) we have

$$\int (\nabla \otimes \mathbf{a}) dV = \oint \mathbf{a} \otimes \mathbf{n} dA \tag{37}$$

where $\otimes$ represents either a gradient, or a divergence, or a curl operation. Applying Eq. 36 to the gradient of the velocity field $\mathbf{u}$ on an auxiliary cell ABCD (see Fig. 2) surrounding the point indexed $j + \frac{1}{2}, k, l$ $(m_\alpha = j)$ yields

$$(\nabla \mathbf{u})_{j+\frac{1}{2},k,l} \mathcal{V}_{j+\frac{1}{2},k,l} = \Big[\mathbf{u}_{j+1,k,l} \mathbf{S}^\xi_{j+1,k,l} - \mathbf{u}_{j,k,l} \mathbf{S}^\xi_{j,k,l} + \mathbf{u}_{j+\frac{1}{2},k+\frac{1}{2},l} \mathbf{S}^\eta_{j+\frac{1}{2},k+\frac{1}{2},l}$$

$$- \mathbf{u}_{j+\frac{1}{2},k-\frac{1}{2},l} \mathbf{S}^\eta_{j+\frac{1}{2},k-\frac{1}{2},l} + \mathbf{u}_{j+\frac{1}{2},k,l+\frac{1}{2}} \mathbf{S}^\zeta_{j+\frac{1}{2},k,l+\frac{1}{2}} - \mathbf{u}_{j+\frac{1}{2},k,l-\frac{1}{2}} \mathbf{S}^\zeta_{j+\frac{1}{2},k,l-\frac{1}{2}} \Big]$$

The expression for the divergence of the velocity field can be obtained in a similar manner. Using these expressions, the final form of the viscous stress tensor at a cell face is

$$
\begin{aligned}
\mathbf{T}_{j+\frac{1}{2},k,l} = \left(\frac{\mu}{\mathcal{V}}\right)_{j+\frac{1}{2},k,l} \Big[& \mathbf{u}_{j+1,k,l}\mathbf{S}^{\xi}_{j+1,k,l} - \mathbf{u}_{j,k,l}\mathbf{S}^{\xi}_{j,k,l} + \mathbf{S}^{\xi}_{j+1,k,l}\mathbf{u}_{j+1,k,l} - \mathbf{S}^{\xi}_{j,k,l}\mathbf{u}_{j,k,l} \\
& -\frac{2}{3}(\mathbf{u}_{j+1,k,l}\cdot\mathbf{S}^{\xi}_{j+1,k,l} - \mathbf{u}_{j,k,l}\cdot\mathbf{S}^{\xi}_{j,k,l})\mathbf{I}\Big] + \left(\frac{\mu}{\mathcal{V}}\right)_{j+\frac{1}{2},k,l}\Big[\mathbf{u}_{j+\frac{1}{2},k+\frac{1}{2},l}\mathbf{S}^{\eta}_{j+\frac{1}{2},k+\frac{1}{2},l} \\
& -\mathbf{u}_{j+\frac{1}{2},k-\frac{1}{2},l}\mathbf{S}^{\eta}_{j+\frac{1}{2},k-\frac{1}{2},l} + \mathbf{u}_{j+\frac{1}{2},k,l+\frac{1}{2}}\mathbf{S}^{\zeta}_{j+\frac{1}{2},k,l+\frac{1}{2}} - \mathbf{u}_{j+\frac{1}{2},k,l-\frac{1}{2}}\mathbf{S}^{\zeta}_{j+\frac{1}{2},k,l-\frac{1}{2}} \\
& +\mathbf{S}^{\eta}_{j+\frac{1}{2},k+\frac{1}{2},l}\mathbf{u}_{j+\frac{1}{2},k+\frac{1}{2},l} - \mathbf{S}^{\eta}_{j+\frac{1}{2},k-\frac{1}{2},l}\mathbf{u}_{j+\frac{1}{2},k-\frac{1}{2},l} + \mathbf{S}^{\zeta}_{j+\frac{1}{2},k,l+\frac{1}{2}}\mathbf{u}_{j+\frac{1}{2},k,l+\frac{1}{2}} \\
& -\mathbf{S}^{\zeta}_{j+\frac{1}{2},k,l-\frac{1}{2}}\mathbf{u}_{j+\frac{1}{2},k,l-\frac{1}{2}} - \frac{2}{3}(\mathbf{u}_{j+\frac{1}{2},k+\frac{1}{2},l}\cdot\mathbf{S}^{\eta}_{j+\frac{1}{2},k+\frac{1}{2},l} - \mathbf{u}_{j+\frac{1}{2},k-\frac{1}{2},l}\cdot\mathbf{S}^{\eta}_{j+\frac{1}{2},k-\frac{1}{2},l} \\
& +\mathbf{u}_{j+\frac{1}{2},k,l+\frac{1}{2}}\cdot\mathbf{S}^{\zeta}_{j+\frac{1}{2},k,l+\frac{1}{2}} - \mathbf{u}_{j+\frac{1}{2},k,l-\frac{1}{2}}\cdot\mathbf{S}^{\zeta}_{j+\frac{1}{2},k,l-\frac{1}{2}})\mathbf{I}\Big]
\end{aligned}
$$

The first term in brackets represents the thin-layer contribution to the viscous flux and the second term in brackets represents the contributions due to the cross-derivatives. The geometrical quantities (volumes and area vectors) in the above expression are simple arithmetic averages. For the scalar and vector fields there are many different ways of doing the averaging. Consider the velocity field **u**. The possible averaging procedures are

$$
\mathbf{u}_{j+\frac{1}{2},k+\frac{1}{2},l} = \begin{cases} \frac{1}{4}\left[\mathbf{u}_{j+1,k,l} + \mathbf{u}_{j+1,k+1,l} + \mathbf{u}_{j,k+1,l} + \mathbf{u}_{j,k,l}\right] \\ \frac{1}{2}\left[\mathbf{u}_{j,k,l} + \mathbf{u}_{j+1,k+1,l}\right] \\ \frac{1}{2}\left[\mathbf{u}_{j+1,k,l} + \mathbf{u}_{j,k+1,l}\right] \end{cases}
$$

The choice of averaging is dictated by diagonal dominance in an implicit scheme. Therefore, for an implicit scheme the last two choices improve diagonal dominance. The criteria for choosing the averaging procedure are given in Ref. 12. The heat flux vector can be derived in a similar manner and the final form of this vector is given by

$$\mathbf{q}_{j+\frac{1}{2},k,l} = -\left(\frac{\kappa}{\mathcal{V}}\right)_{j+\frac{1}{2},k,l}\left[T_{j+1,k,l}\mathbf{S}^{\xi}_{j+1,k,l} - T_{j,k,l}\mathbf{S}^{\xi}_{j,k,l}\right] -$$

$$\left(\frac{\kappa}{\mathcal{V}}\right)_{j+\frac{1}{2},k,l}\left[T_{j+\frac{1}{2},k+\frac{1}{2},l}\mathbf{S}^{\eta}_{j+\frac{1}{2},k+\frac{1}{2},l} - T_{j+\frac{1}{2},k-\frac{1}{2},l}\mathbf{S}^{\eta}_{j+\frac{1}{2},k-\frac{1}{2},l}\right.$$

$$\left.+T_{j+\frac{1}{2},k,l+\frac{1}{2}}\mathbf{S}^{\zeta}_{j+\frac{1}{2},k,l+\frac{1}{2}} - T_{j+\frac{1}{2},k,l-\frac{1}{2}}\mathbf{S}^{\zeta}_{j+\frac{1}{2},k,l-\frac{1}{2}}\right]$$

The viscous numerical fluxes for the other faces and directions can be derived in a similar manner.

(c) Temporal differencing:

So far, the time-differencing part of the algorithm was not addressed because we considered only the semi-discrete conservation law. If Δt represents the time steps, then the temporal term of Eq. 16 is represented as

$$\frac{d}{dt}\int_{\mathcal{V}(t)} Q dV = \frac{\mathcal{V}_{j,k,l}}{\Delta t}\left[(1+\omega)\Delta^n Q_{j,k,l} - \omega\Delta^{n-1}Q_{j,k,l}\right]$$

where $\Delta^n Q_{j,k,l} = Q^{n+1}_{j,k,l} - Q^n_{j,k,l}$ and ω controls the temporal accuracy of this representation. For example, if $\omega = 0$ we have first-order temporal accuracy and if $\omega = \frac{1}{2}$ we have second-order temporal accuracy.

Algorithm

Using the concepts developed in the preceding sections, the numerical algorithm is written as a two-parameter family of implicit and explicit schemes.

$$\Delta^n Q_{j,k,l} + \frac{\Delta t}{\mathcal{V}_{j,k,l}}\frac{\theta}{(1+\omega)}\left[\sum_{\alpha=1}^{n_d}(\hat{F}^{\alpha,n+1}_{m_\alpha+\frac{1}{2}} - \hat{F}^{\alpha,n+1}_{m_\alpha-\frac{1}{2}}) - \mathcal{V}_{j,k,l}\hat{W}^{n+1}_{j,k,l}\right] =$$

$$\frac{\omega}{(1+\omega)}\Delta^{n-1}Q_{j,k,l} - \frac{\Delta t}{\mathcal{V}_{j,k,l}}\frac{(1-\theta)}{(1+\omega)}\sum_{\alpha=1}^{n_d}(\hat{F}^{\alpha,n}_{m_\alpha+\frac{1}{2}} - \hat{F}^{\alpha,n}_{m_\alpha-\frac{1}{2}}) - \mathcal{V}_{j,k,l}\hat{W}^{n}_{j,k,l}\Big] \qquad (38)$$

where $\theta = 0$ defines an explicit scheme and $\theta \neq 0$ defines an implicit scheme. Further, second-order temporal accuracy is achieved only when $\theta = \omega + \frac{1}{2}$. In the present study we concentrate only on implicit schemes. Before considering the actual solution procedure we assume that the grid is invariant in time, *i.e.*, $\mathbf{v} = 0$. This also implies that the geometrical parameters such as the volume and surface area vectors are invariant in time.

The usual method of solving the nonlinear difference equation is through time linearization, *i.e.*, the nonlinear equation is linearized about the known state Q^n and the linear system of equations is solved using known techniques. This approach suffers from linearization errors. In order to avoid linearization errors a Newton method is used[12]. As an analogy consider a simple nonlinear equation $f(x) = 0$. The Newton method for this equation is

$$f'(x^k)(x^{k+1} - x^k) = -f(x^k) \qquad k = 1, 2, ...$$

In the nonlinear difference equation represented by Eq. 38, Q^{n+1} is the unknown quantity. Let q^p be an approximation to Q^{n+1} such that as p increases, q^p approaches Q^{n+1}. Linearizing Eq. 38 about the known state q^p we have

$$\left[\mathrm{I} + \frac{\Delta t}{\mathcal{V}_{j,k,l}}\frac{\theta}{(1+\omega)}(\sum_{\alpha=1}^{n_d}\delta_\alpha\frac{\partial\hat{F}}{\partial q} - \mathcal{V}_{j,k,l}\frac{\partial\hat{W}}{\partial q})\right]^p \Delta^p q = -(q^p_{j,k,l} - Q^n_{j,k,l}) -$$

$$\frac{\Delta t}{\mathcal{V}_{j,k,l}}\frac{\theta}{(1+\omega)}\left[\sum_{\alpha=1}^{n_d}(\hat{F}^{\alpha,p}_{m_\alpha+\frac{1}{2}} - \hat{F}^{\alpha,p}_{m_\alpha-\frac{1}{2}}) - \mathcal{V}_{j,k,l}\hat{W}^{p}_{j,k,l}\right] + \frac{\omega}{(1+\omega)}\Delta^{n-1}Q_{j,k,l} -$$

$$\frac{\Delta t}{\mathcal{V}_{j,k,l}}\frac{(1-\theta)}{(1+\omega)}\left[\sum_{\alpha=1}^{n_d}(\hat{F}^{\alpha,n}_{m_\alpha+\frac{1}{2}} - \hat{F}^{\alpha,n}_{m_\alpha-\frac{1}{2}}) - \mathcal{V}_{j,k,l}\hat{W}^{n}_{j,k,l}\right] \tag{38}$$

where $\Delta^p q = q^{p+1} - q^p$ and $\delta_\alpha() = ()_{m_\alpha+\frac{1}{2}} - ()_{m_\alpha-\frac{1}{2}}$ similarly the other terms. If $q^0 = Q^n$ and only one subiteration is carried out then we have the usual noniterative algorithm. The LHS of the algorithm can be simplified by considering only a spatially first-order accurate scheme. Even so, when the subiterations converge, the RHS is satisfied to the desired accuracy. We also assume that eigenvalues and eigenvectors are independent of q^p. Using the one-sided representation of the inviscid numerical flux, Eq. 33, and making using of the fact that $\sum_f \mathbf{S}^f = 0$ for a closed cell, we get

$$\left[\mathbf{I} - \Delta t\theta\frac{\partial\hat{W}}{\partial q}\right]\Delta^p q + \frac{\Delta t}{\mathcal{V}_{j,k,l}}\frac{\theta}{(1+\omega)}\Bigg[\mathbf{A}^{\xi,+}_{j-\frac{1}{2}}(\Delta^p q_j - \Delta^p q_{j-1}) +$$
$$\mathbf{A}^{\xi,-}_{j+\frac{1}{2}}(\Delta^p q_{j+1} - \Delta^p q_j) + \mathbf{A}^{\eta,+}_{k-\frac{1}{2}}(\Delta^p q_k - \Delta^p q_{k-1}) + \mathbf{A}^{\eta,-}_{k+\frac{1}{2}}(\Delta^p q_{k+1} - \Delta^p q_k) +$$
$$\mathbf{A}^{\zeta,+}_{j-\frac{1}{2}}(\Delta^p q_l - \Delta^p q_{l-1}) + \mathbf{A}^{\zeta,-}_{j+\frac{1}{2}}(\Delta^p q_{l+1} - \Delta^p q_l)\Bigg]^p = \text{RHS(Eq. 39)} \tag{40}$$

The above equation is too large to solve on the computer and hence needs to be simplified. There are several options available to us. The first of these is to use a Gauss-Seidel relaxation in the predominant stream direction.[12] Let this direction be the j-direction. We then drop the $j-1$ and $j+1$ terms to obtain

$$\left[\mathbf{I} - \Delta t\theta\frac{\partial\hat{W}}{\partial q} + \frac{\Delta t}{\mathcal{V}_{j,k,l}}\frac{\theta}{(1+\omega)}(\mathbf{A}^{\xi,+}_{j-\frac{1}{2}} - \mathbf{A}^{\xi,-}_{j+\frac{1}{2}})\right]^p \Delta^p q_j +$$
$$\frac{\Delta t}{\mathcal{V}_{j,k,l}}\frac{\theta}{(1+\omega)}\Bigg[\mathbf{A}^{\eta,+}_{k-\frac{1}{2}}(\Delta^p q_k - \Delta^p q_{k-1}) + \mathbf{A}^{\eta,-}_{k+\frac{1}{2}}(\Delta^p q_{k+1} - \Delta^p q_k) +$$
$$\mathbf{A}^{\zeta,+}_{j-\frac{1}{2}}(\Delta^p q_l - \Delta^p q_{l-1}) + \mathbf{A}^{\zeta,-}_{j+\frac{1}{2}}(\Delta^p q_{l+1} - \Delta^p q_l)\Bigg]^p = \text{RHS(Eq. 39)} \tag{41}$$

This equation is still too large to solve and is now impemented in an approximately factorized form. First define the operator $\hat{\mathbf{A}}$ as

$$\hat{\mathbf{A}}^{\xi} = \left[\mathbf{I} - \Delta t \theta \frac{\partial \hat{W}}{\partial q} + \frac{\Delta t}{\mathcal{V}_{j,k,l}} \frac{\theta}{(1+\omega)} (\mathbf{A}^{\xi,+}_{j-\frac{1}{2}} - \mathbf{A}^{\xi,-}_{j+\frac{1}{2}})\right] \tag{42}$$

Then the approximately factorized scheme is

$$\left[\hat{\mathbf{A}}^{\xi} + \frac{\Delta t}{\mathcal{V}_{j,k,l}} \frac{\theta}{(1+\omega)} (\mathbf{A}^{\eta,+}\delta^{b}_{\eta} + \mathbf{A}^{\eta,-}\delta^{f}_{\eta})\right]^{p}$$

$$(\hat{\mathbf{A}}^{\xi})^{-1} \left[\hat{\mathbf{A}}^{\xi} + \frac{\Delta t}{\mathcal{V}_{j,k,l}} \frac{\theta}{(1+\omega)} (\mathbf{A}^{\zeta,+}\delta^{b}_{\zeta} + \mathbf{A}^{\zeta,-}\delta^{f}_{\zeta})\right]^{p} \Delta^{p} q_{j} = \text{RHS(Eq. 39)} \tag{43}$$

The operators δ^{b} amd δ^{f} represent the conventional backward and forward difference operators, respectively. Equation 43 is the final form of the algorithm which is implemented in the computer code. In its present form the algorithm is for three-dimensional flows. For a two-dimensional flow there is no approximate factorization and the algorithm reduces to the following line-relaxation algorithm

$$\left[\hat{\mathbf{A}}^{\xi} + \frac{\Delta t}{\mathcal{V}_{j,k,l}} \frac{\theta}{(1+\omega)} (\mathbf{A}^{\eta,+}\delta^{b}_{\eta} + \mathbf{A}^{\eta,-}\delta^{f}_{\eta})\right]^{p} \Delta^{p} q_{j} = \text{RHS(Eq. 39)} \tag{44}$$

For a one-dimensional flow this further reduces to apoint-relaxation scheme given by

$$\hat{\mathbf{A}}^{\xi,p} \Delta^{p} q_{j} = \text{RHS(Eq. 39)} \tag{45}$$

Note that for the two- and three-dimensional cases the operators represent block-tridiagonal systems of equations where the order of the block matrices is n_e. The one-dimensional case involves the inversion of a full matrix of order n_e.

Boundary Conditions

The discussion in this section is only applicable to external flows. For such a situation, the typical computational domain(s) (see Fig. 3) are bounded by (i) an inflow boundary, (ii) an outflow boundary, (iii) a wall boundary, (iv) a freestream boundary, and (v) a symmetry boundary. There are additional special cases to consider such as (i) a geometrically singular boundary (axis), and (ii) zonal or overlap boundaries. Each of these boundary conditions is discussed below:

Inflow Boundary

For the types of flows of interest, the inflow boundary is assumed to be in the freestream and Dirichlet boundary conditions are implemented implicitly. A special case of this boundary condition occurs in the three-dimensional flow around blunt bodies where the entire face collapses into a line. Such a boundary has to be treated with special care as it has been known to have caused problems in other three-dimensional calculations. This boundary is discussed later in this section. For a freestream inflow we have

$$Q^{n+1}_{1,k,l} = Q_\infty \qquad \forall n, k, l$$

Outflow Boundary

In the this research effort, the outflow is assumed to be supersonic and hence a simple zeroth/first extrapolation of flow variables is done. This can be implemented implicitly. The extrapolation causes some error in the subsonic layer close to the wall. However, past experience has shown that this effect is negligible. This is expressed mathematically as

$$Q^{n+1}_{NJ,k,l} = Q^{n+1}_{NJ-1,k,l} \qquad \forall n, k, l$$

Wall Boundary

The wall is assumed to noncatalytic, *i.e.*, $\mathbf{n} \cdot \nabla c_s = 0$. Further the wall is assumed to be a isothermal with a fixed wall temperature T_w which in principle can vary from point to point on the surface. No slip conditions $\mathbf{u} = \mathbf{0}$ are also implemented at the wall. Assuming no-slip condition at the wall leaves us with only the pressure to be estimated at the wall. Assuming near boundary-layer behavior at the wall, this pressure is obtained by zeroth order extrapolation from the interior. Strictly speaking, the value of the wall pressure should be determined by solving the normal momentum equation.[7] In the present case this is not done.

The implementation of the wall boundary condition is quite involved. The layer of cells close to the wall have indices $j, 2, l$ and cells indexed $j, 1, l$ are fictitious cells (see Fig. 4). The values of the flow variables in these cells are determined from the simple relations given below

$$\mathbf{u}^{n+1}_{j,1,l} = -\mathbf{u}^{n+1}_{j,2,l}$$

$$T^{n+1}_{j,1,l} = 2T_w - T^{n+1}_{j,2,l}$$

$$p^{n+1}_{j,1,l} = p_w = p^{n+1}_{j,2,l}$$

In evaluating the viscous stresses, one sided differences are used at the wall.

Freestream Boundary

Like the inflow boundary, at the freestream boundary Dirichlet conditions are used implicitly in the code. This far field boundary condition assumes that all flow discontinuities are contained well within this boundary.

$$Q^{n+1}_{j,NK,l} = Q_\infty \qquad \forall n, j, l$$

Symmetry Boundary

The three-dimensional geometry considered in this research are assumed to possess a plane of symmetry. Across this plane of symmetry, all flow quantities are reflected. These reflection boundary conditions are implemented implicitly and are expressed as

$$U^{n+1}_{j,k,NL} = U^{n+1}_{j,k,NL+1} \qquad U = \rho_s, \rho, p, T, E, u, v$$

$$w^{n+1}_{j,k,NL} = -w^{n+1}_{j,k,NL+1}$$

$$U^{n+1}_{j,k,1} = U^{n+1}_{j,k,0} \qquad U = \rho_s, \rho, p, T, E, u, v$$

$$w^{n+1}_{j,k,1} = -w^{n+1}_{j,k,0} \qquad U = \rho_s, \rho, p, T, E$$

Axis Boundary[13]

This boundary condition is perhaps the most difficult one to implement. It must be emphasized here that a geometric singularity does not imply that the flow variables are singular. There is some respite from this singularity in the finite-volume method because the cell centers done not coincide with the axis (see Fig. 5). In the present analysis it is assumed that the grid is sufficiently smooth in the neighborhood of the singularity. First we write the semidiscrete version of Eq. 1 for a cell indexed $1, k, l$. However the state Q considered is assumed to be located at $5/6, k, l$ where

$$Q_{\frac{5}{6},k,l} = \frac{5}{6}Q_{1,k,l} + \frac{1}{6}Q_{2,k,l}$$

a similar conservation equation can be written for the call indexed $Q_{2,k,l}$. Using this equation, $Q_{2,k,l}$ can be eliminated from the conservation equation for the cell indexed $Q_{1,k,l}$. The variables required for the higher-order flux corrections are obtained from cells that are diametrically opposite to the cell being considered (see Fig. 5). This is probably the single most important requirement. In this effort we generate grids such that the singular axis is enclosed in a cylindrical tube extending two cell widths. This reduces the requirement of interpolation to obtain the state vector at diametrically opposite locations.

Overlap Boundary

Dirichlet boundary conditions are used at overlap boundaries. The values of Q from one grid are transferred to another through the overlap region. If the overlapping regions do not exactly match then we have to use interpolation to transfer the values. The tranferred values are assumed to remain constant during the subiteration.

Finally, it must be noted that low order boundary conditions are used in the implicit part of the algorithm. These boundary conditions are explicitly corrected to second-order accuracy at the end of every subiteration, inasmuch as the left hand side goes to zero at convergence. We are also investigating the possibility of using characteristic boundary conditions.

Code Development

Before delving into the details of the new multidimensional code for reacting flows, the important aspect of grid generation has to be addressed. This is discussed next.

(a) Grid Generation:

The grid required by the new code is always three-dimensional irrespective of the dimensionality of the flow being computed. For a one-dimensional flow the grid is a tube of a unit square cross-section and for a two-dimensional flow the grid is a slab of unit depth. The reason for this is that a three-dimensional grid is necessary to compute the surface area vectors and cell volumes required by the finite-volume approach. In doing so one removes conditionality (which slows down the code) and the grid can be treated the same way for all flows. The price paid in this approach is increased storage for the one- and two-dimensional cases. In the present research, however, the very important aspect of grid generation is kept independent of the code, *i.e.*, the reacting flow code does not include any grid generation package. This makes the code more flexible and applicable to a variety of problems and faster at the same time.

Now the code to integrate the equations is divided into three codes; a pre-processor, an integrator, and a post-processor. Each of these codes is discussed below.

(b) Preprocessor:

The basic unit in the integration of the equations is a sequence. A sequence can contain one or more finite-volume grids. Currently, these grids have to have a continuous overlap. For example, in the case of hypersonic flow past a wedge, one can have two sequences; the first sequence consisting of a single grid around the forebody and the second sequence containing two grids in the wake. Each sequence can have its own spatial and temporal accuracy. For the example of the wedge, the forebody sequence can have first-order temporal and second-order spatial accuracy, while the aftbody sequence can have second-order temporal and spatial accuracy.

The function of the preprocessor is to set up the datasets and files necessary for the integration package. The preprocessor reads the flow conditions, the species set and the number of reactions. The program then gets the species thermodynamic, transport and reaction data from the database. Currently, the data base contains the species O_2, N_2, NO, NO^+, O, N, and e^-. The thermodynamic data are in the form cubic-spline coefficients. Using these data the code sets up the reference conditions required for nondimensionalization. The number of sequences is then read in along with the pertinent accuarcy information. The coordinates of the grids that form the sequences are also read in. Based on these coordinates the surface area vectors and cell volumes are computed and written into files and the flow variables are initizalized at two time levels. The details of the reference conditions and file structure are written into the preprocessor output file which is read by the integration package.

(c) Integrator:

This is the main code of the three and is a FORTRAN implementation of the algorithm shown in Eq. 43. It is in this code that the flow equations are actually integrated. The integration package reads in the reference conditions and file structure from the preprocessor file. Note that the integration package does not read in the grid coordinates but reads in the cell surface area vectors and volumes instead. This saves both computational time and storage since the area vectors and volumes are not computed over and over again and the grid coordinates are not stored. This assumes that the grids used in the computation are invariant in time. If at later date dynamic adpative gridding is desired then this code will have to be modified.

It must be noted here that the boundary condition procedures are also not integral to the code. The code provides hooks for boundary conditions and it is up to the user to write the boundary condition procedures and routines. This was done in order to make the code flexible. Datasets in the code's native format and residual history are the only outputs from the integration package. These datasets and histories are analyzed by the postprocessor which is discussed next.

(d) Postprocessor

The main function of the postprocessor is to analyze the flowfield datasets computed by the integration package. The postprocessor computes the various fields like pressure, temperature, Mach number, etc. for purpose of graphical representation. The most important function of the postprocessor is the computation of the aerothermal loads.

The postprocessor computes the heat-transfer and aerodynamic coefficients. The postprocessor can also be used for creating files for the purpose of computing radiation intensities and transport.

Results

(a) Model Problem

In order to test the feasiblity of the numerical method outlined in the preceding sections, a model problem was solved. This model problem is shown below in the integral form

$$\frac{d}{dt}\int_{\mathcal{V}(t)} udV + \oint_{\partial\mathcal{V}(t)} (\omega u + \psi\frac{u^2}{2})dA = \mu\oint_{\partial\mathcal{V}(t)} \frac{\partial u}{\partial x}dA + \kappa\int_{\mathcal{V}(t)} u(u-\frac{1}{2})(u-1)dV \qquad (46)$$

where $\omega, \psi, \mu, \kappa$ are constants. The second term on the left hand side of the equation represents the advection term. The first and second terms on the right hand side represent the viscous and source terms, respectively. The model problem is actually Burgers equation and in the differential form is

$$\frac{\partial u}{\partial t} + \frac{\partial}{\partial x}(\omega u + \psi\frac{u^2}{2}) = \mu\frac{\partial^2 u}{\partial x^2} + \kappa u(u-\frac{1}{2})(u-1)$$

Equation 46 represents many problems and of these a few representative problems have been selected. These are

Problem 1: The first model problem solved was that of steady, inviscid, non-reacting flow, *i.e.*, $\omega = 0$, $\mu = \kappa = 0$, and $\psi = 1$. Mathematically stated,

$$\frac{\partial u}{\partial t} + \frac{\partial}{\partial x}(\frac{u^2}{2}) = 0$$

subject to the following initial and boundary conditions

$$u(x,0) = 1 - 2x \quad 0 \le x \le 1, \qquad u(0,t) = 1, u(1,t) = -1 \quad 0 \le t < \infty$$

The exact solution to the above problem is

$$u(x,t) = \begin{cases} 1 & 0 \le x < 0.5 \\ -1 & 0.5 < x \le 1 \end{cases}$$

which means that there is a stationary shock located at $x = 0.5$. This case was computed using a CFL number of 1×10^6. The calculations converged within four steps and the results are shown in Fig. 6. It is evident that discontinuity that develops can be captured without oscillations within two to three cells. Such crisp capture is due to the upwind nature of the scheme.

Problem 2: The second model problem solved was that of unsteady, inviscid, non-reacting flow. This was to check the time-accuracy (especially important in the calculation of unsteady flows) of the algorithm. The problem statement is identical to the the one above except that the initial and boundary conditions are changed. Specifically, the initial and boundary conditions used are

$$u(x,0) = \begin{cases} 1 & 0 \le x < 0.3 \\ 0 & 0.3 < x \le 1 \end{cases} \qquad u(0,t) = 1 \quad t \ge 0$$

The exact solution to the above problem is of a discontinuity travelling to the right with a speed of stopped at $t = 0.6$, the discontinuity would be located at $x = 0.6$. The results of this calculation are shown in Fig. 7. The figure clearly shows that the shock is tracked nearly perfectly.

Problem 3:[14] The third model problem solved was that of unsteady, inviscid, reacting flow. This was to check the influence of the source term on the calculation. The source term is somewhat contrived in the sense that it does not represent the actual source term of a chemically reacting system. The initial and boundary conditions used are the same as in the previous problem. The problem has been solved for various values of the source term strength κ. The results of this calculation are shown in Figs. 8a-8f. Several important conclusions can be made from these computations. For small values of κ, there is little or no influence on the solution. The source term tends to sharpen the discontinuity. When the source term reaches a critical value the discontinuity does not move very far from its initial position. It is unlikely that this situation will be encountered in the actual chemically reacting problem. A high source term strength translates to near equilibrium conditions. For such a situation it is not a good idea to use the nonequilibrium code to compute the equilibrium flow - one has to use a code dedicated to computing the equilibrium flow.

Problem 4: The final model problem solved was that of steady, viscous, reacting and non-reacting flow. For the non-reacting case, the exact solution of the problem is known. The computed solution and the corresponding convergence history are shown in Figs. 9a-9b. Note that the reaction term again sharpens the gradient.

These four model problems clearly demonstrate the feasilbity and accuracy of the algorithm. The FORTRAN code developed for the actual chemically reacting system is currently being tested for a variety of problems. The results of these calculations will be presented at a later date.

Concluding Remarks

The equations governing the reacting flow of a multicomponent gas have been derived. These equations are applicable to one-, two- and three-dimensional flows. The various modelling assumptions and expressions have been detailed. A numerical scheme based on the finite-volume method has been developed to solve the governing equations. The various methods of representing the inviscid and viscous numerical fluxes have been detailed. The algorithm is spatially second order accurate (third order accuracy can be achieved in principle) and temporally second-order accurate. This temporal accuracy can be reduced to first order for cases where a steady state solution is required. The feasibility and accuracy of the algorithm hace been demonstrated for some simple one-dimensional model problems. For the actual problem of multi-dimensional chemically reacting flows, the algorithm has been implemented as a set of three computer codes - a preprocessor, an integrator, and a postprocessor. The code is cu-urently being debugged and tested for simple geometrical shapes in two dimensions. Once the code has been validated for the simpler cases, it will be used to compute the complete unsteady reacting flow field around the Aeroassist Flight Experiment (AFE) body shape.

References

[1] P. A. Thompson, Compressible Fluid Dynamics, McGraw-Hill Book Co., New York, 1972.

[2] C. Park, Nonequilibrium Hypersonic Aerodynamics, John Wiley and Sons, New York, 1990.

[3] Y. Liu and M. Vinokur, ``Equilibrium Gas Flow Computations I: Accurate and Efficient Calculation of Equilibrium Gas Properties,'' NASA Contractor Report (in preparation).

[4] R. L. Jaffe, ``The Calculations of High Temperature Equilibrium and Nonequilibrium Specific Heat Data for N_2, O_2 and NO,'' AIAA Paper No. 87-1633, June 1987.

[5] F. G. Blottner, M. Johnson, and M. Ellis, ``Chemically Reacting Viscous Flow Program for Multi-Component Gas Mixtures,'' Report No. SC-RR-70-754, Sandia Laboratories, Albuquerque, New Mexico, Dec. 1971.

[6] C. R. Wilke, ``A Viscosity Equation for Gas Mixtures,'' *J. Chem. Phys.*, Vol. 18, No. 4, Apr. 1950, p. 517.

[7] M. Vinokur, ``An Analysis of Finite-Difference and Finite-Volume Formulations of Conservation Laws,'' NASA CR-177416, June 1986.

[8] B. van Leer, ``Towards the Ultimate Conservation Difference Scheme V, A Second-Order Sequel to Godunov's Method,'' *J. Comp. Phys.*, Vol. 54, 1979, pp. 174-201.

[9] S. K. Godunov, ``A Finite-Difference Method for the Numerical Computation of Non-linear Discontinuous of the Equations of Fluid Dynamics,'' *Math. Sb.*, Vol. 47, 1959, pp. 357-393.

[10] P. L. Roe, ``Approximate Riemann Solvers, Parameter Vectors, and Difference Schemes,'' *J. Comp. Phys.*, Vol. 43, 1981, pp. 357-372.

[11] A. Harten, ``On a Class of High Resolution Total-Variation Stable Finite-Difference Schemes,'' *SIAM J. Num. Anal.*, Vol. 21, 1984, pp. 1-23.

[12] S. Chakravarthy and K. Y. Szema, ``An Euler Solver for Three Dimensional Supersonic Flows with Subsonic Pockets,'' AIAA Paper No. 85-1703, Jan. 1986.

[13] M. Vinokur, *Private Communication*, Jun. 1988.

[14] H. C. Yee, ``A Class of High-Resolution Explicit and Implicit Shock Capturing Methods,'' NASA TM-101088, Feb. 1989.

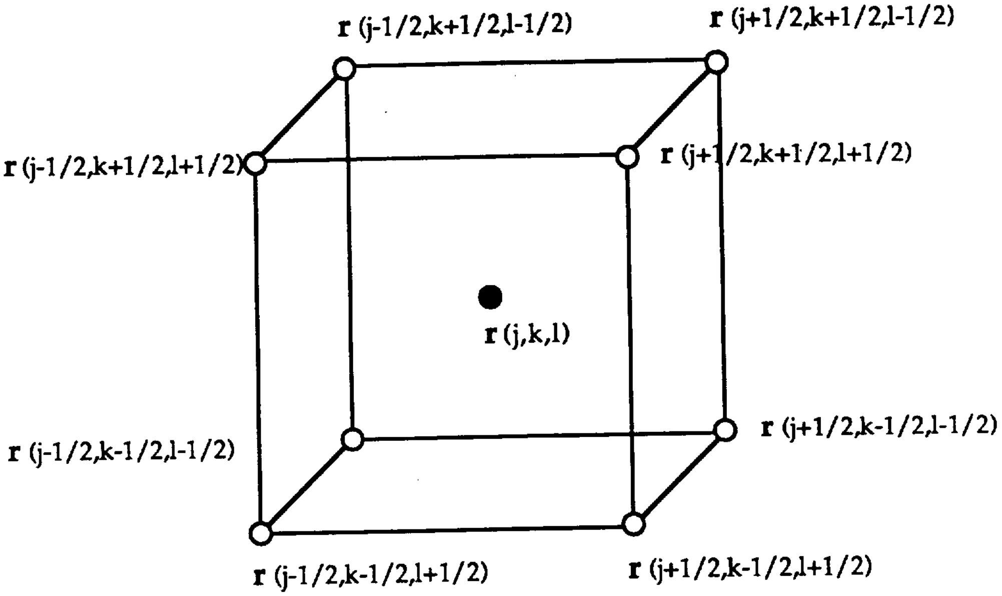

Figure 1. Typical finite volume cell showing cell corners (open circles) and cell center (solid circle)

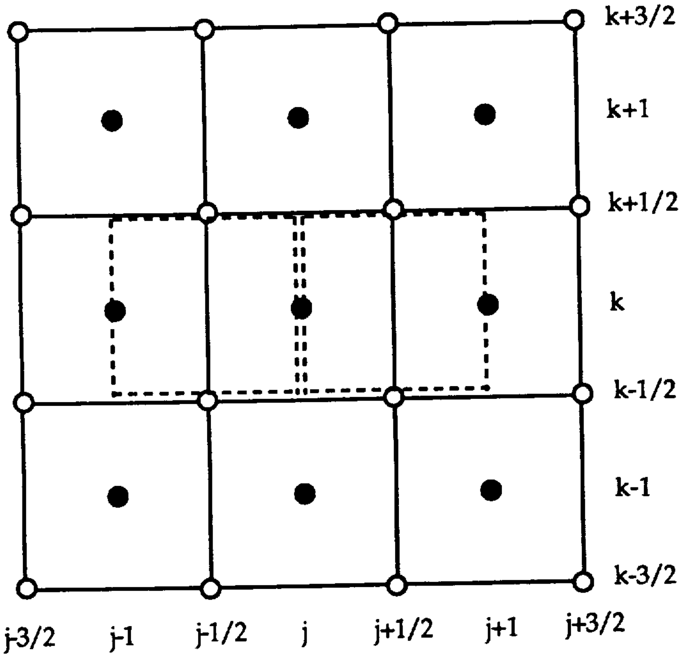

Figure 2. Secondary grid for transport calculations

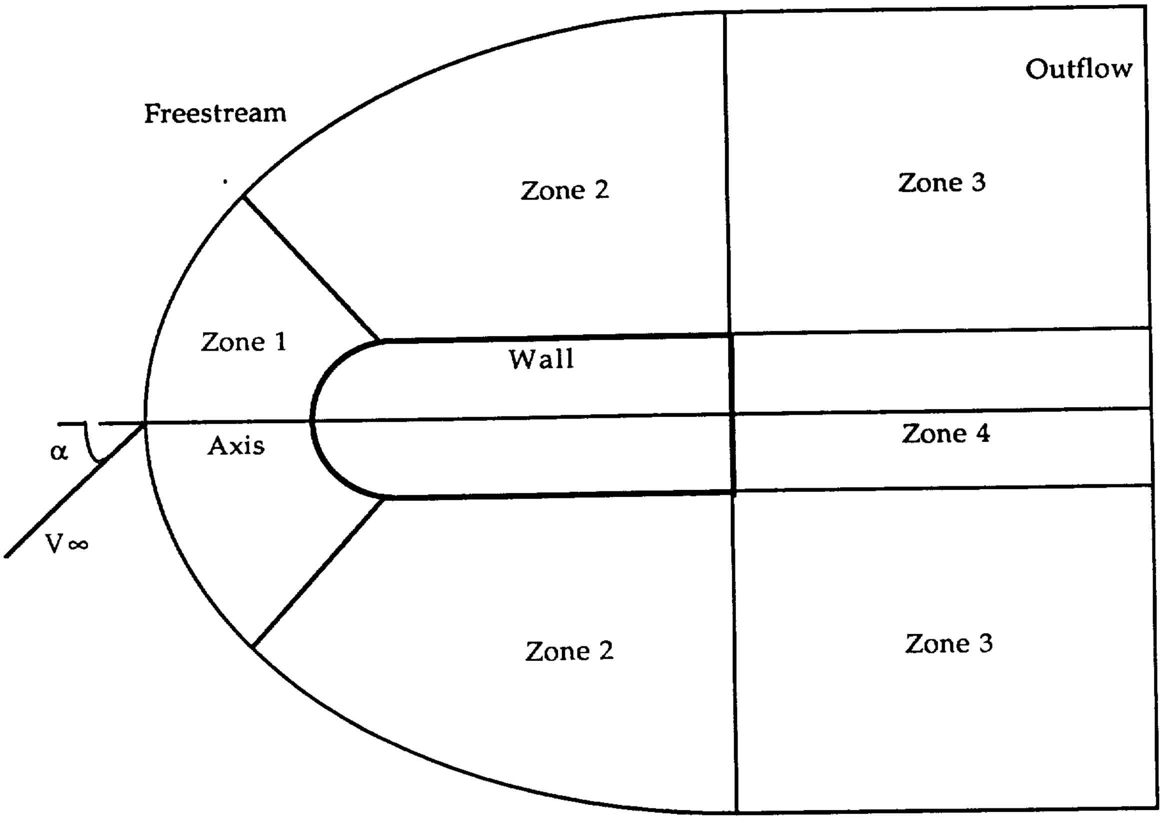

Figure 3. Typical multiple grid system for external flows

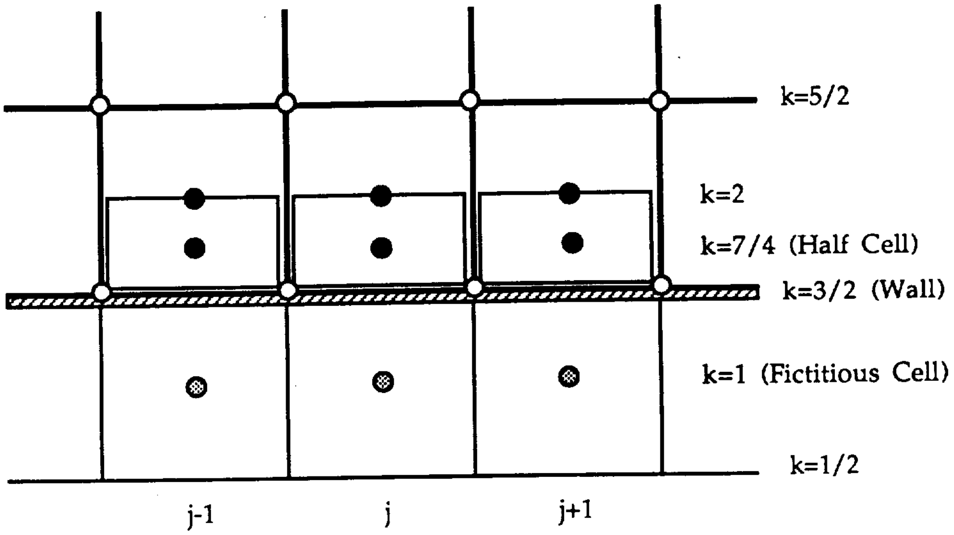

Figure 4. Wall cell and half cell geometry in the l plane

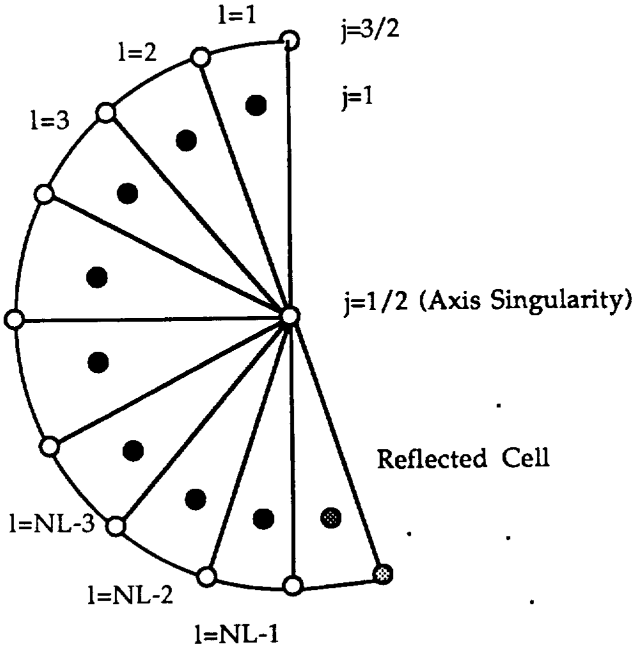

Figure 5. Cell configuration at the singular axis as seen end on

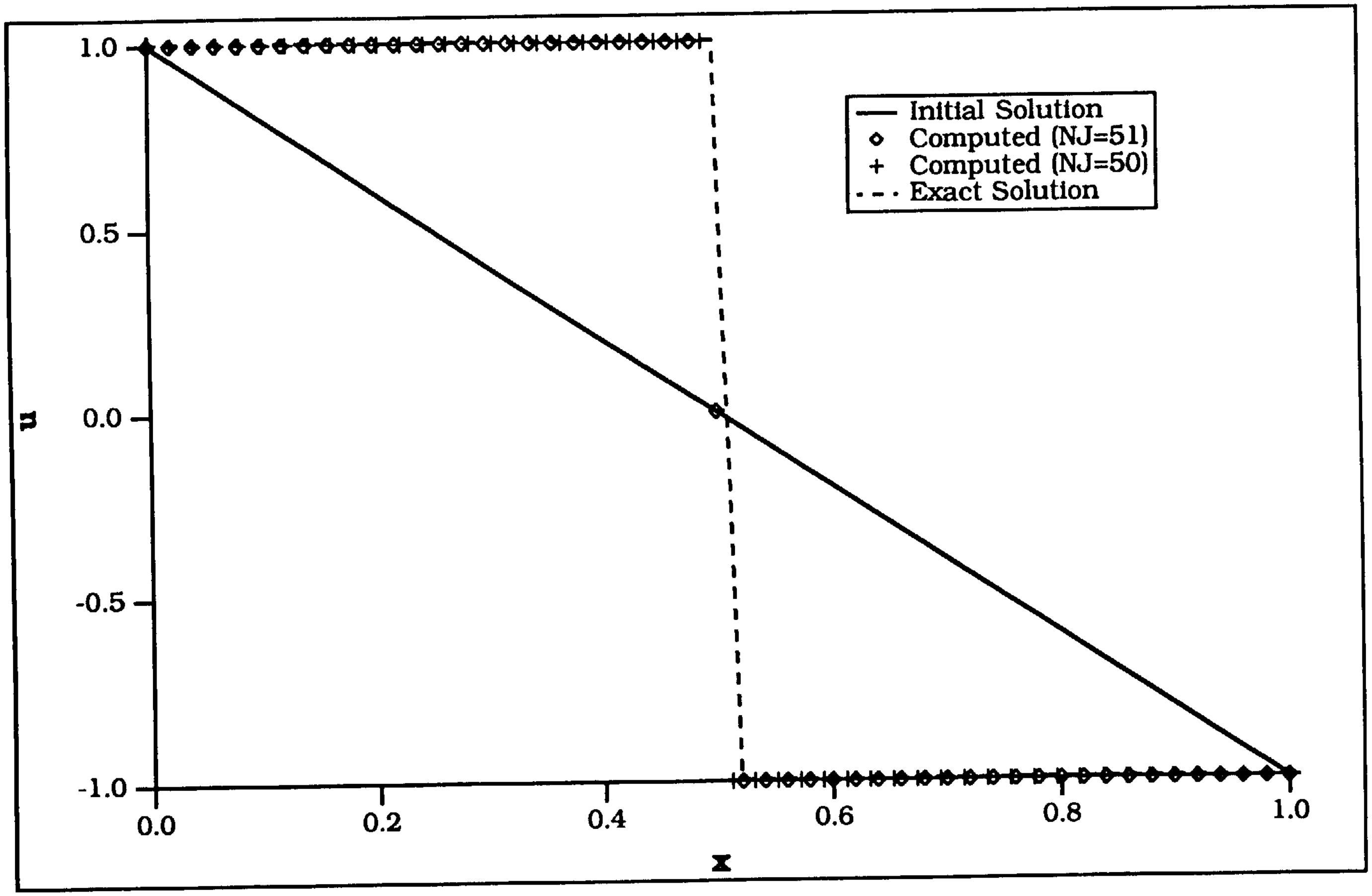

Figure 6. Steady, inviscid Burgers' equation solution

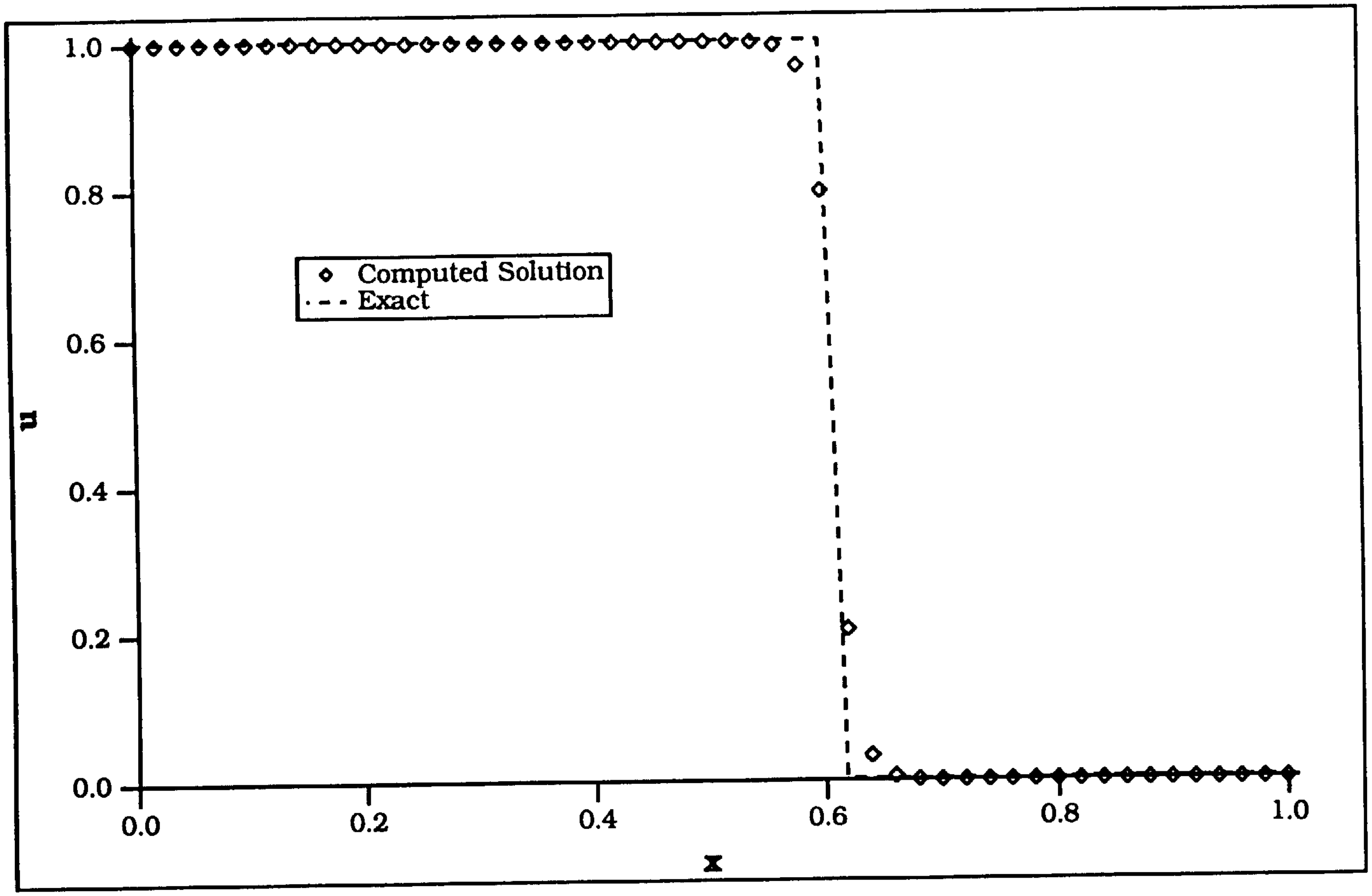

Figure 7. Shock tracking problem solution at t=0.6

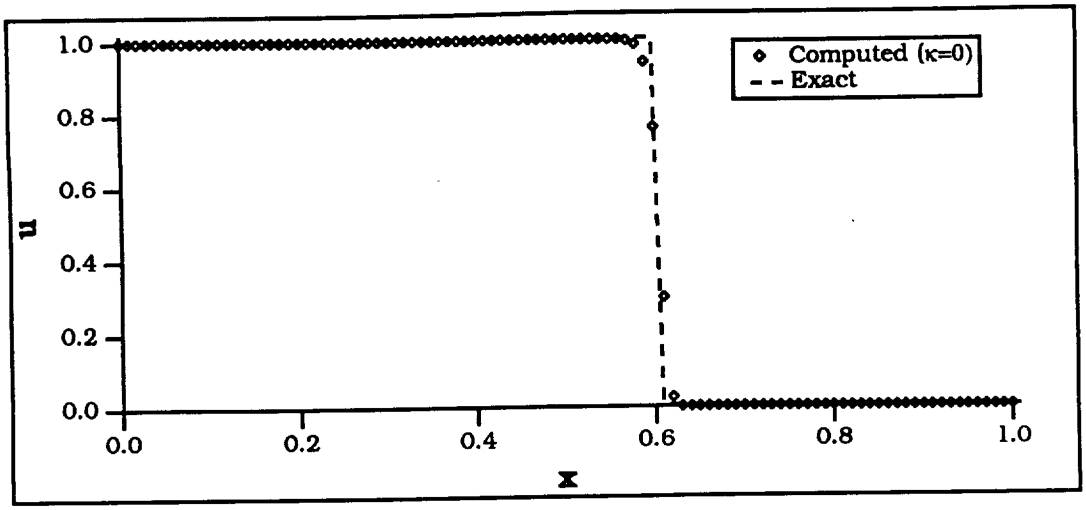

Figure 8a. Solution with no source term.

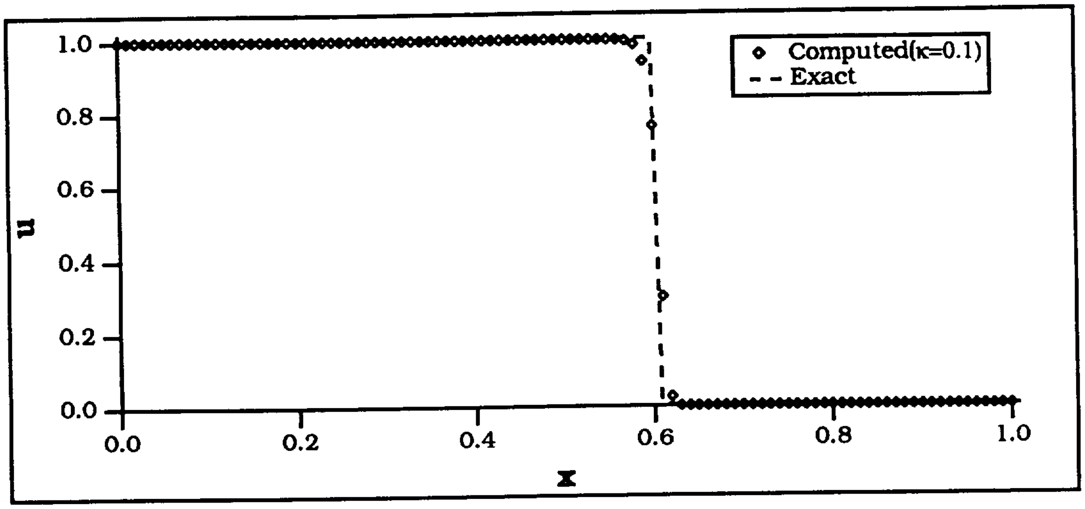

Figure 8b. Solution with source term strength=0.1

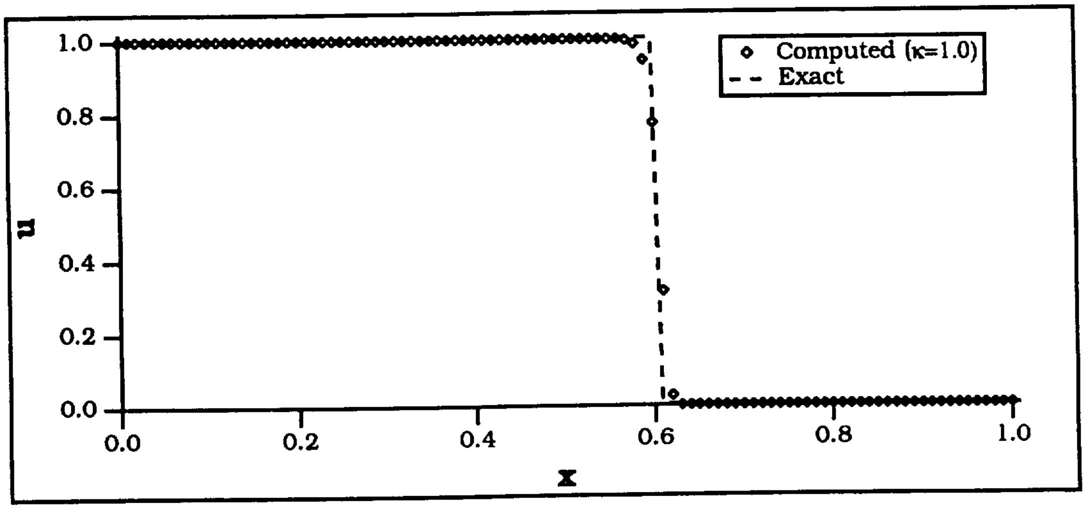

Figure 8c. Solution with source term strength=1.0

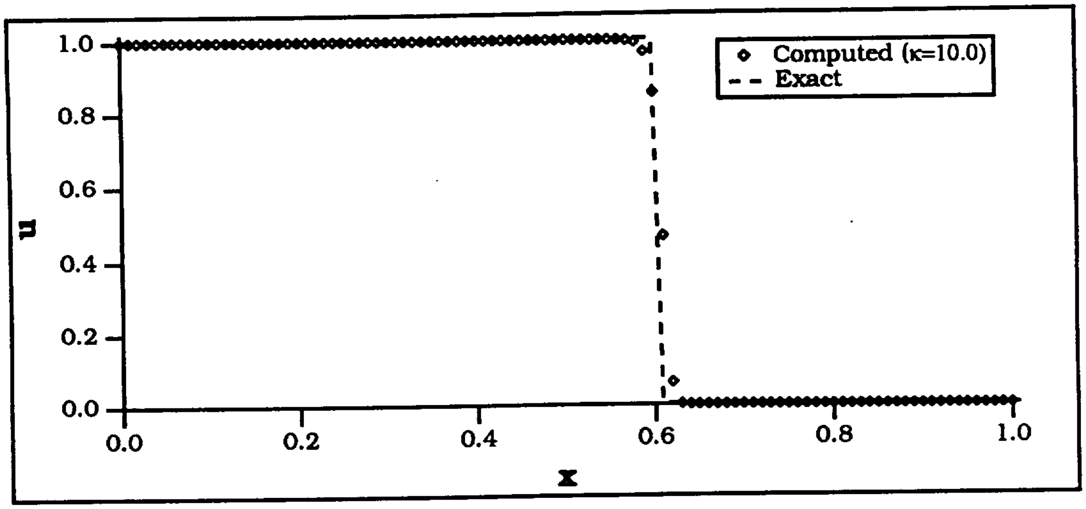

Figure 8d. Solution with source strength=10.0

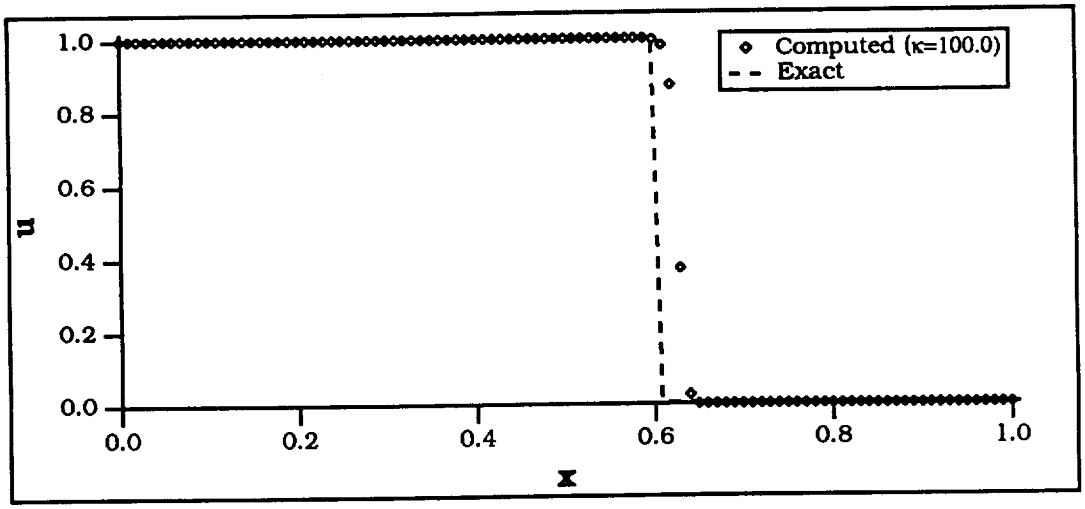

Figure 8e. Solution with source strength=100.0

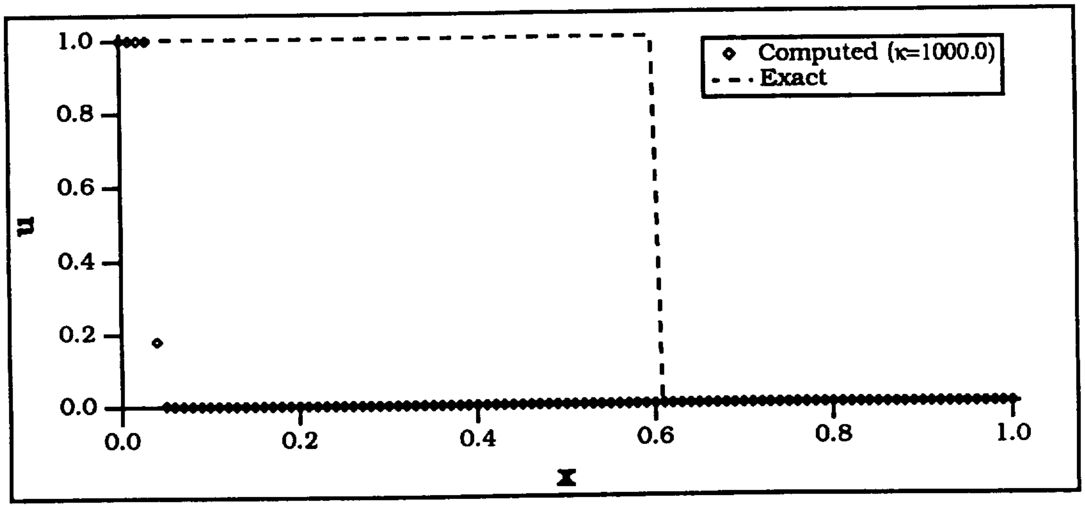

Figure 8f. Solution with source strength=1000.0

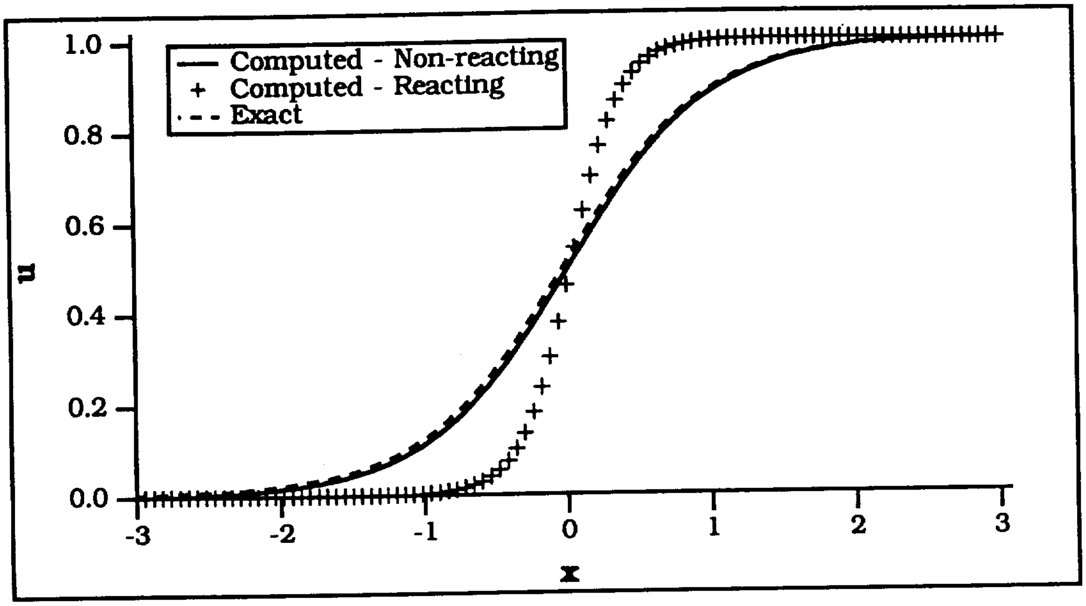

Figure 9a. Solution of the viscous, non-reacting problem

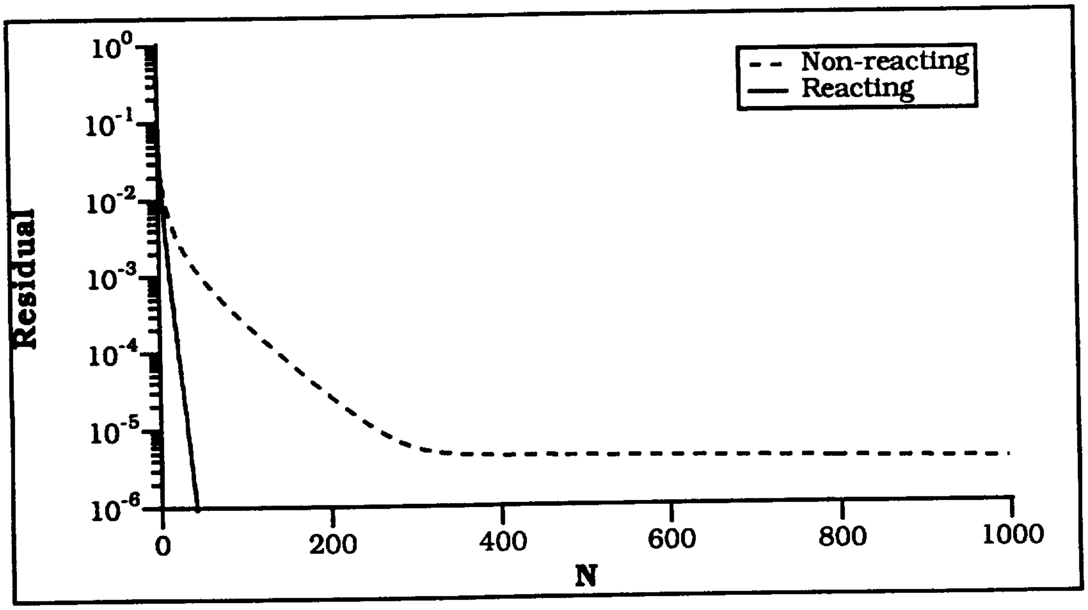

Figure 9b. Convergence history